Martinez-Felipe, A.; Badia, J.; Santonja Blasco, L.; Imrie, C.; Ribes Greus, MD. (2013). A kinetic study of the formation of smectic phases in novel liquid crystal ionogens. European Polymer Journal. 49(6):1553-1563. doi:10.116/j.eurpolymj.2013.01.021.

Elsevier Editorial System(tm) for European Polymer Journal
Manuscript Draft

Manuscript Number:

Title: A kinetic study of the formation of smectic phases in novel liquid crystal ionogens

Article Type: Research Paper

Section/Category:

Keywords: Liquid crystal polymers (LCP); Differential scanning calorimetry (DSC); non-isothermal melt-crystallisation kinetic analysis

Corresponding Author: Professor Amparo Ribes-Greus, Ph. D.

Corresponding Author's Institution: Universidad Politécnica de Valencia

First Author: Alfonso Martínez-Felipe, Dr.

Order of Authors: Alfonso Martínez-Felipe, Dr.; José D Badia, Dr.; Laura Santonja-Blasco, M.Sc; Corrie T Imrie, Professor; Amparo Ribes-Greus, Ph. D.

Abstract: The non-isothermal kinetic analysis of the isotropic-melt to liquid crystalline phase transition of novel liquid crystalline ionogenic copolymers, LCI, the 10-(4-methoxyazobenzene-4'-oxy)decyl methacrylate]-co-2-(acrylamido-2-methyl-1-propanesulfonic acid)s, 10-MeOAzB/AMPS, copolymers, has been performed based on calorimetric experiments at different cooling rates. A classical non-isothermal crystallisation methodology, based on Avrami's equations, was applied and it has shown that the formation of the mesophases from the isotropic state occurred close to the thermodynamic equilibrium and can be described with high accuracy by using different kinetic parameters. The results evidence the presence of several individual processes in the formation of liquid crystalline phases from the melt and a strong dependence of phase transition rates and activation energies with acid contents. In addition, the decrease in the phase transition rate is related to a decrease in orientational entropy and the final inhibition of the liquid crystal behaviour is ascribed to an exponential increase in the activation energy of the phase transition, promoted by strong acid aggregation. An optimum composition of the 10-MeOAzB/AMPS copolymers to achieve the dual characteristics of LCI (ionogenic and liquid crystalline behaviour) requires acid concentrations capable of promoting structure-forming effects on the LC phases and the evolution of phase separated morphologies.

Suggested Reviewers: Stephen J Picken Professor
Professor, Department of Chemical Engineering, Delft University of Technology
S.J.Picken@tudelft.nl
Expertise in liquid crystalline structures

Andrew G. Cook Doctor
Department of Chemistry, University of Reading
a.g.cook@reading.ac.uk
Expert in liquid crystalline transitions

Juozas V. Grazulevicius Professor
Professor, Organic Technology, Kaunas University of Technology

juozas.grazulevicius@ktu.lt
Broad experience in properties of liquid crystal materials

Salvador Montserrat-Ribas Professor
Maquinas y Motores Térmicos, Universitat Politècnica de Catalunya
montserrat@mmt.upc.edu
Expert in calorimetric measurements on complex polymeric systems

Angels Serra i Albet Professor
Organic Chemistry, Universitat rovira i Virgili
angels.serra@urv.cat
Expertise in liquid crystalline chemistry and characterisation of polymers

Valencia, 24th January 2012

Dear Editor:

I have submitted a manuscript entitled "**A kinetic study of the formation of smectic phases in novel liquid crystal ionogens**" for consideration for publication in the **European Polymer Journal**. The manuscript describes the melt-liquid crystal transition of a set of novel liquid crystal side chain copolymers containing sulfonic acid groups having application potential as anisotropic polymer electrolyte membranes. Due to the relevance of the structure-properties relations in these materials, it is important to describe the successive processes involved in the formation of the mesomorphic templates from the isotropic phase. The study of the non-isothermal calorimetric transition carried out in this paper has proved to be useful to describe the forming role of the acid groups on the stabilisation of the liquid crystal phase.

The manuscript contains original material which has not been published nor is being considered for publication elsewhere.

I look forward to hearing from you in due course.

Yours faithfully,

Prof. Amparo Ribes Greus
Institute of Materials Technology

*Graphical Abstract

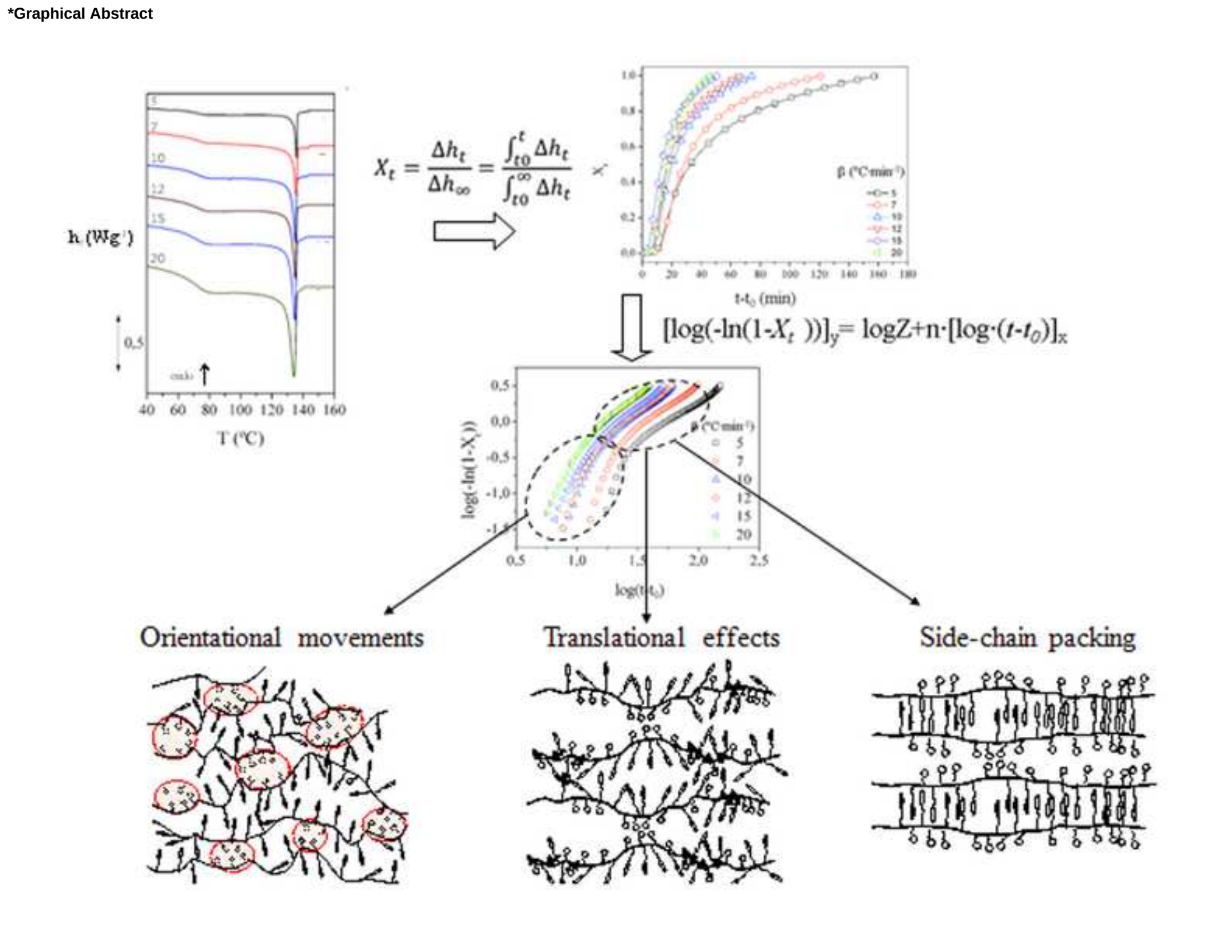

Highlights

Kinetic phase transition analysis of side-chain LC polymers containing acid groups

Nematic suppression in copolymers by orientational restrictions

Non-isothermal kinetic analysis of the isotropic to liquid crystal transition

Activation energies increase exponentially when acid aggregation occurs

Role of structure forming sulfonic acid groups in liquid crystals

Captions to Figures

Figure 1. Schematic representation of the methodology followed for the study of the non-isothermal isotropic-liquid crystal phase transition of the **10-MeOAzB/AMPS** copolymers.

Figure 2. DSC cooling traces of **P10-MeOAzB** (*Cop - 1/0*) obtained at different cooling rates, β, from 5 to 20 ºC/min.

Figure 3. Phenomenological and kinetic analysis of the isotropic-nematic phase transition shown by **P10-MeOAzB**: a) X_t curves; b) Avrami plots.

Figure 4. (a) DSC traces recorded at cooling rates, β = 5 and 20 ºC·min^{-1} and (b) the dependence of X_t on $\phi(t)$ for the **10-MeOAzB/AMPS** copolymers. Experimental points have not been shown for the sake of clarity.

Figure 5. (a) T_c values; (b) $\tau_{1/2}$; (c) ξ values (**Eq. 2**) for the **10-MeOAzB/AMPS** copolymers:

Figure 6. The dependence of the entropy change associated with the isotropic-liquid crystal phase transition ($\Delta S_c/R$) measured for differing cooling rates on the composition of the **10-MeOAzB/AMPS** copolymers. For the homopolymer we see an isotropic-nematic-smectic A transition while the copolymers exhibit an isotropic-smectic A transition

Figure 7. Calculation of the activation energy of the isotropic-smectic A process for the **10-MeOAzB/AMPS** copolymers (Ea_{Tc}). Plots of the (a) Kissinger, (b) Flynn-Wall-Ozawa methods; (c) Evolution of Ea_{Tc} for the two methods with the composition.

Figure 8. Examples of Avrami plots obtained for the phase transition of the **10-MeOAzB/AMPS** copolymers at high and low cooling rates. High (a) and intermediate (b) 10-MeOAzB concentrations

Figure 9. Schematic representation of the isotropic –melt to liquid crystalline transitions in the P10-MeOAzB (a), **P10-MeOAzB/AMPS** copolymers showing liquid crystal behaviour (b) and amorphous **P10-MeOAzB/AMPS** copolymers (c)

A kinetic study of the formation of smectic phases in novel liquid crystal ionogens

[1]A. Martínez-Felipe; [1]J.D. Badía, [1]L. Santonja-Blasco; [2]C.T. Imrie; [1,*]A. Ribes-Greus

[1]Institute of Materials Technology, Universitat Politècnica de València, Camino de Vera S/N, 46022 Valencia, Spain

[2]Chemistry, School of Natural and Computing Sciences, Meston Building, University of Aberdeen, Aberdeen AB24 3UE Aberdeen, Scotland (UK).

*corresponding author: A. Ribes-Greus, e-mail: aribes@ter.upv.es

Abstract

The non-isothermal kinetic analysis of the isotropic-melt to liquid crystalline phase transition of novel liquid crystalline ionogenic copolymers, LCI, the 10-(4-methoxyazobenzene-4'-oxy)decyl methacrylate]-co-2-(acrylamido-2-methyl-1-propanesulfonic acid)s, **10-MeOAzB/AMPS**, copolymers, has been performed based on calorimetric experiments at different cooling rates. A classical non-isothermal crystallisation methodology, based on Avrami's equations, was applied and it has shown that the formation of the mesophases from the isotropic state occurred close to the thermodynamic equilibrium and can be described with high accuracy by using different kinetic parameters. The results evidence the presence of several individual processes in the formation of liquid crystalline phases from the melt and a strong dependence of phase transition rates and activation energies with acid contents. In addition, the decrease in the phase transition rate is related to a decrease in orientational entropy and the final inhibition of the liquid crystal behaviour is ascribed to an exponential increase in the activation energy of the phase transition, promoted by strong acid aggregation. An optimum composition of the 10-MeOAzB/AMPS copolymers to achieve the dual characteristics of LCI (ionogenic and liquid crystalline behaviour) requires acid concentrations capable of promoting structure-forming effects on the LC phases and the evolution of phase separated morphologies.

Keywords

Liquid crystal polymers (LCP), Differential scanning calorimetry (DSC), non-isothermal melt-crystallisation kinetic analysis

1. Introduction

Side chain liquid crystal polymers (SCLCP) exhibit a unique duality of properties combining those of low molar mass liquid crystals with those of polymers. This combination of properties arises from the structure of SCLCPs in which the mesogenic groups are covalently attached as pendants to a polymer backbone *via* a flexible spacer. The role of the flexible spacer is to decouple, at least to some extent, the relative tendencies of the mesogenic groups to self-assemble and form the liquid crystal phase from those of the polymer backbone to adopt random coil configurations [**1**]. The incorporation of nonmesogenic units along the backbone allows for additional functionalities to be endowed upon the polymer [**2-4**] Of particular interest in recent years have been SCLCPs containing ionic and ionogenic units and these are also referred to as liquid crystal ionomers and iononogens (LCI). This interest stems not only from their considerable application potential in a range of quite diverse areas but perhaps most notably as anisotropic electrolytes, but also because they provide a demanding challenge to our understanding of self-assembly in polymeric systems [**5, 6**].

We recently reported the synthesis and phase behaviour of the 10-(4-methoxyazobenzene-4'-oxy)decyl methacrylate]-co-2-(acrylamido-2-methyl-1-propanesulfonic acid)s, copolymers (**1**),

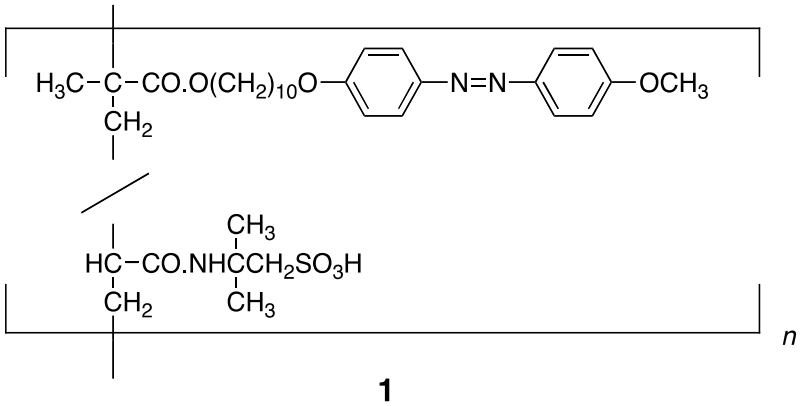

1

and refer to them using the acronym **10-MeOAzB/AMPS** in which 10-MeOAzB refers to the liquid crystal side chain and AMPS to the sulfonic acid-based group. These copolymers exhibited smectic A phase behaviour over a broad range of compositions, specifically for copolymers containing 0.45 or greater mol fraction of 10-MeOAzB side chains [**7**]. This observation, in itself, is not unusual and may be accounted for by a compression of the backbone in the plane perpendicular to the liquid crystal director which enhances the

interactions between the mesogenic groups. Surprisingly, however, the smectic A-isotropic transition did not simply decrease on increasing the AMPS mol fraction but instead appeared to reach a limiting value. Such effect was accompanied by changes in the structure of the smectic A phase on increasing the AMPS mol fraction and this was attributed, at least in part, to hydrogen bonding between the sulfonic acid groups. In addition, a phase separated structure was observed consisting of regions of smectic A phase and acid-rich domains.

It appears therefore that the sulfonic acid groups play a central structure-forming role in determining the phase behaviour of these copolymers. Due to the relevance that processing conditions may have on the preparation of materials and membranes with liquid crystalline templates from the melt, this work investigates with more detail the structural formation of the smectic A phase from the isotropic melt for the **10-MeOAzB/AMPS** copolymers. To achieve this we performed a calorimetric kinetic study of the non-isothermal isotropic melt-liquid crystal phase transition for the homopolymer (**P10-MeOAzB**) and the **10-MeOAzB/AMPS** copolymers. A classical non-isothermal crystallisation approach has been used, based on Avrami's equations and methods [**8, 9, 10**]. We note that such characterisation technique may be successful to determine accurately the lower enthalpy/entropy changes occurring during the transitions from the isotropic state to the mesophases and also between mesophases in low-ordered liquid crystal phases (such as nematic or some smectic phases) [**11 – 22**].

2. Experimental

The synthesis of the 10-MeOAzB/AMPS copolymers was performed by free radical copolymerisation of the monomers, using 1,1'-azobis(cyclohexane carbonitrile) as the initiator in dimethyl formamide (DMF), as has been described in detail elsewhere [**7**, **11**]. The isotropic melt-liquid crystal transition kinetics were investigated using differential scanning calorimetry (DSC), by means of non-isothermal linear temperature-time programs. The DSC thermograms were obtained using a Mettler Toledo DSC 822^e analyser (Columbus, OH, USA) and samples of around 5 mg. The thermal program consisted of alternating heating and cooling scans. An initial heating scan from 25 to 180ºC was applied to ensure the sample had entered the isotropic phase so deleting any thermal history. Subsequently, the samples were submitted to alternating cooling scans (with rate β = 5, 7, 10, 12, 15 and 20 ºC·min^{-1}) and heating scans (with rate β = 10 ºC·min^{-1}) between 0 and 180 ºC. All the thermograms were obtained under a nitrogen atmosphere and using an intracooler for temperature control (Haake EK90/mt). The STAR^e 9.2 software was used to obtain the experimental calorimetric parameters. All the experiments were performed at least three times and the averages and standard deviations of the thermodynamic parameters were obtained.

DSC Phenomenological analysis [10]

The isotropic-liquid crystal phase transitions of the copolymers were analysed using the methodology and equations shown in **Figure 1**. First, the specific enthalpy change associated with the isotropic-liquid crystal phase transition was calculated by integrating the DSC curves obtained in the cooling scan along the time axis (ΔH_t). The fraction of liquid crystal phase at time t (X_t) was obtained by normalising the ΔH_t, values with respect to the enthalpy change corresponding to the complete isotropic-liquid crystal transition (ΔH_∞), following **Eq 1**, ranging from X_{t-0}= 0 (isotropic phase) to $X_{t-\infty}$ = 1 (liquid crystal phase). The half-time of the formation of the liquid crystal phase ($\tau_{1/2}$) was defined as the time at which X_t = 0.5. The phase transition temperature (T_c) was taken to be the minimum of the exotherm. The phenomenological analysis was completed by calculating the so-called phase transition rate parameter, ξ, which in this case actually corresponds to the rate of formation of the liquid crystal phase, defined as the slope of the plots of the variable $(\tau_{1/2} \cdot T_c)^{-1}$ against the cooling rate, β (**Eq. 2**).

Kinetic analysis of the isotropic-liquid crystal phase transition

The study of the bulk isotropic-liquid crystal phase transition of the copolymers was completed by calculating the apparent activation energy (Ea_{Tc}). The Kissinger [**12**] and the Flynn-Wall-Ozawa [**13, 14**] integral methods were applied at the maximum rate of the formation of the liquid crystal phase. The values of $\ln(\beta \cdot T_c^{-2})$ and $\log(\beta)$, respectively, were represented versus T_c^{-1} (**Eq 3** and **4**, respectively), and Ea_{Tc} was calculated from the slopes of the curves.

In addition, the development of multiple individual processes occurring at the isotropic-liquid crystal transition was investigated by applying Avrami's equations to the X_c data [**8, 9**]. The time-dependent probability of the formation of LC domains during the isotropic-liquid crystal transition can be then described by **Eq. 5** in which t_0 corresponds to the onset of the transition. The logarithmic form (**Eq.6**) allows for a linear fit of the phase transition data versus time. In order to consider the effect of the non-mesogenic units in the copolymers, **Eq. 6** was corrected, to give **Eq. 7**, in which $1-\lambda(\infty)$ is the weight fraction of the polymer potentially liquid crystalline at the termination of the process [**15**]. The parameter $1-\lambda(\infty)$, was calculated as the ratio of the ΔH_∞ values of the copolymers with respect to the homopolymer, at each cooling rate. Two empirical parameters can be obtained from the Avrami analysis for each DSC cooling curve, Z and n, which describe the mechanism of the isotropic-liquid crystal transition processes. From these values, it is possible to calculate a rate parameter $k = Z^{(1/n)}$ (**Eq. 8**), which describes the speed of the formation of the liquid crystal phase for each individual process.

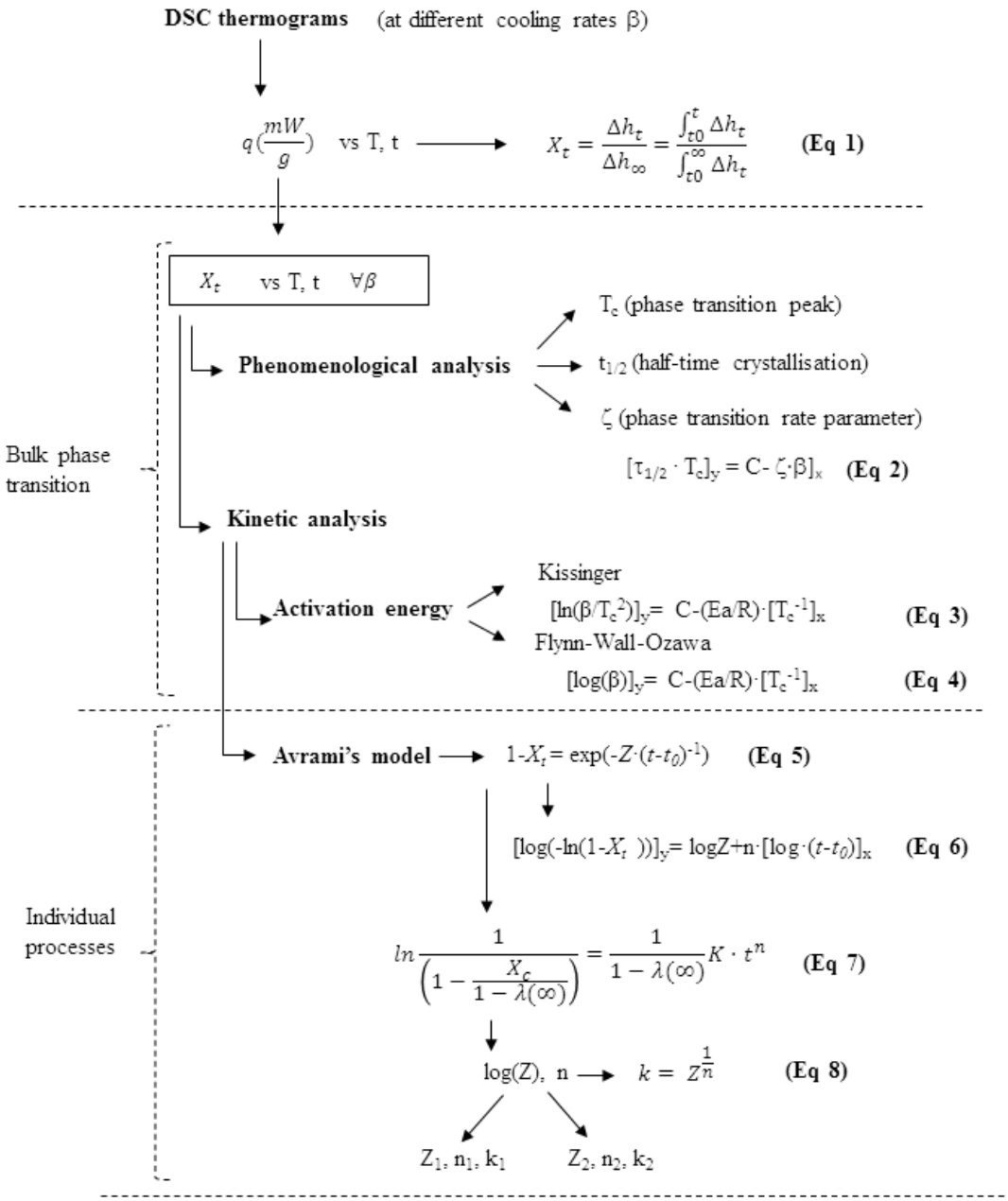

Figure 1. Schematic representation of the methodology followed for the study of the non-isothermal isotropic-liquid crystal phase transition of the **10-MeOAzB/AMPS** copolymers.

3. Results and discussion

3.1 Kinetic analysis of the isotropic-nematic-smectic A phase transition of the homopolymer P10-MeOAzB (*Cop-1/0*)

Figure 2 shows the non-isothermal isotropic melt-liquid crystal exotherms for the **P10-MeOAzB** homopolymer (*Cop-1/0*) at six different cooling rates. All the DSC traces contain two distinct events: a first order exothermic transition at high temperatures (T_c ~ 134 - 136ºC), associated with the isotropic-nematic phase transition, and a glass transition at lower temperatures (T_g ~ 71 - 74ºC) [**4**]. We have shown previously using polarised optical microscopy and small angle X-ray diffraction that on cooling from the isotropic phase, **P10-MeOAzB** forms a narrow temperature range nematic phase and on further cooling, a smectic phase.

The temperature corresponding to the minimum of the exothermic peak (T_c), and the associated enthalpy (ΔH_c) and entropy (ΔS_c) changes measured at different cooling rates are listed in **Table 1**. The values of T_c, ΔH_c and ΔS_c measured at β = -10 ºC·min^{-1} are in good agreement with those reported elsewhere [**4, 7, 16, 17**]. On increasing the cooling rate, the isotropic-nematic transition exotherm becomes broader and shifts to slightly lower temperatures. The extent of supercooling is reproducible but very small (ΔT < 2ºC) when the cooling rate is varied between 5 and 20ºC/min, suggesting that the transition occurs close to the thermodynamic equilibrium [**10**]. This observation is consistent with a thermodynamically weak transition such as a nematic-isotropic transition.

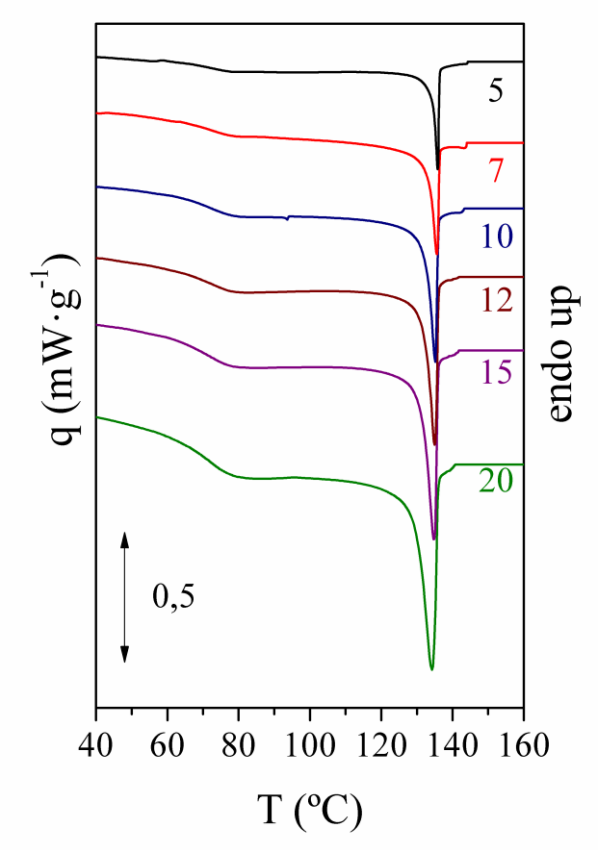

Figure 2. DSC cooling traces of **P10-MeOAzB** (*Cop - 1/0*) obtained at different cooling rates, β, from 5 to 20 ºC/min.

The quantitative analysis of the non-isothermal isotropic-liquid crystal phase transition of **P10-MeOAzB** involved the calculation of the liquid crystal fraction (X_t) as a function of time, $\phi(t) = t - t_0$, using **Eq. 1**. The dependence of X_t on $\phi(t)$ is shown in **Figure 3a** revealing sigmoidal plots, which can be understood as reminiscent of autocatalytic processes [**10**]. The values of apparent total phase transition period, $\Delta t_c = t_{\phi=0.99} - t_{\phi=0.01}$, and half-phase transition time, $\tau_{1/2}$, were obtained from the X_i curves, and are listed in **Table 2**. **Figure 3a** clearly shows the differences in the transitional process of **P10-MeOAzB** seen on varying the cooling rate. Specifically, the shift of the X_t curves towards smaller $\phi(t)$ values on increasing β and the correspondingly lower Δt_c and $\tau_{1/2}$ values, reveal that isotropic-liquid crystal phase transition takes place more rapidly at higher cooling rates. Only a slight deviation is noted for β=15 and 20 ºC/min at low ϕ_t. Similar observations are usually explained by more pronounced supercooling at higher cooling rates, promoting polymer crystallisation at temperatures more displaced from equilibrium (T_c^0). It appears reasonable to assume that a similar explanation accounts for the behaviour of the isotropic-liquid crystal phase transition, although we note that

the extent of supercooling is small. A value of ξ = 5.14·10^{-3} K^{-1} was calculated for **P10-MeOAzB** using **Eq. 2**.

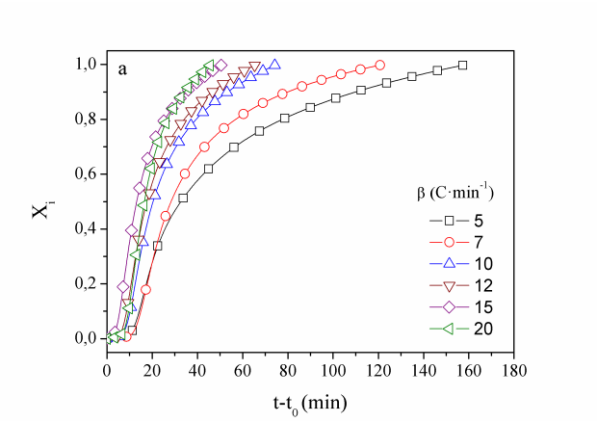

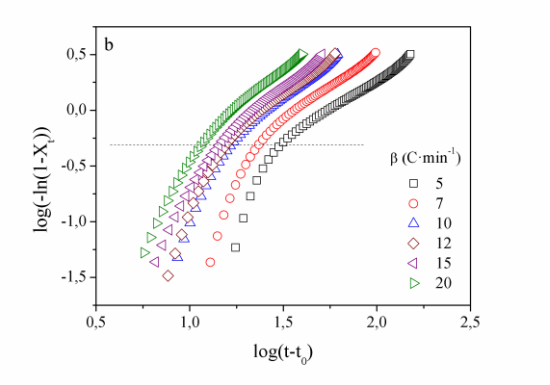

Figure 3. Phenomenological and kinetic analysis of the isotropic-nematic phase transition shown by **P10-MeOAzB**: a) X_t curves; b) Avrami plots.

The Avrami plots for the isotropic-nematic phase transition of **P10-MeOAzB** obtained using **Eq. 5** and **7** are shown in **Figure 3b**. Each of these plots contains two distinct linear regions revealing the occurrence of a primary process (hereinafter, **P1**), at short transition times, and a secondary process (hereinafter, **P2**), at longer times. We suggest that these two processes could be assigned to the isotropic-nematic (**P1**) and nematic-smectic A (**P2**) transitions of the homopolymer, respectively [**16, 17**].

From the logarithmic representations of the two individual curves, the Avrami kinetic parameters related to the primary (*Z1*, *n1*, *k1*) and secondary (*Z2*, *n2*, *k2*) processes were obtained, according to **Eq. 7** and **8**, and are given in **Table 3**. The high R^2 values indicate that the two transition processes are well described by the Avrami model. It is also noteworthy that the Avrami rate constants for **P10-MeOAzB**, k_i, are of the same order of magnitude as seen for

anisotropic crystallisable polymers (~10^{-2} s^{-1}) [**18, 19**]. The slightly higher rates and *n* values seen for **P10-MeOAzB** may presumably be attributed to the morphological differences between the formation of ordered crystalline phases and transitions involving mesophases [**20**]. The differences in *n* and ln(Z) for the two processes may be interpreted in terms of differences in the mechanisms associated with **P1** and **P2**. Higher Avrami exponents and rate constants are found for **P1** (*n1 > n2; k1 > k2*), suggesting that the isotropic-nematic transition occurs more rapidly that the nematic-smectic A transition.

3.2 Kinetic analysis of the isotropic-smectic A transition for the 10-MeOAzB/AMPS-*x/y* copolymers

3.2.1 Bulk transition properties

Figure 4 shows the DSC cooling scans of the copolymers recorded at the lowest and highest cooling rates, namely, β = 5 and β = 20 ºC·min^{-1}, distinguishing non-isothermal isotropic melt-liquid crystal transition exotherms and glass transitions, T_g. Phase assignation was carried out on the basis of polarised optical microscopy and small angle x-ray diffraction studies [**7**]. The DSC traces measured at intermediate values of β are essentially identical and fall between these limiting curves.

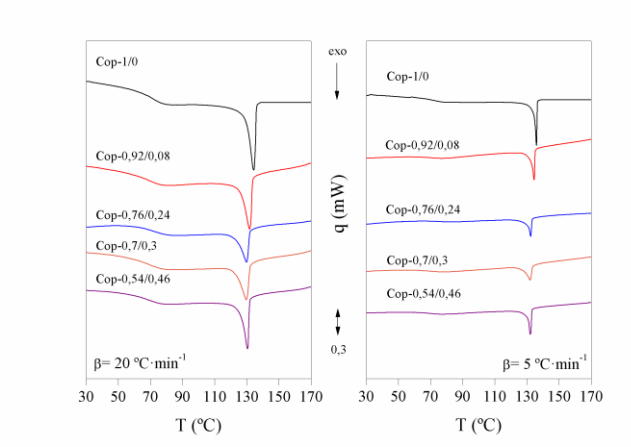

a

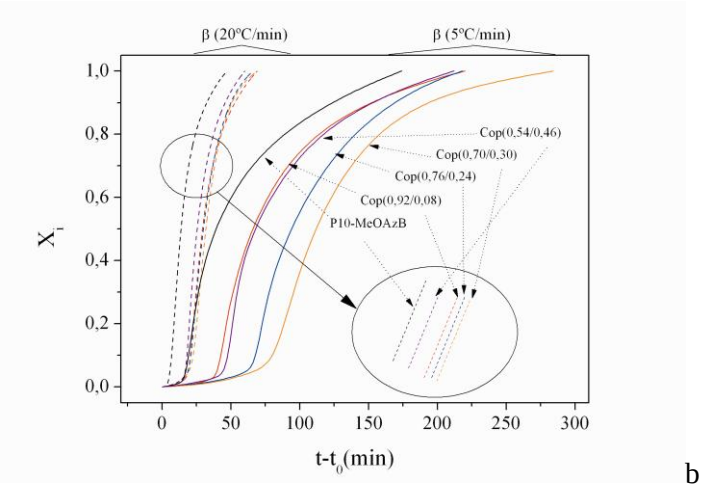

b

Figure 4. (a) DSC traces recorded at cooling rates, β = 5 and 20 ºC·min^{-1} and (b) the dependence of X_t on $\phi(t)$ for the **10-MeOAzB/AMPS** copolymers. Experimental points have not been shown for the sake of clarity.

The calorimetric parameters (T_c, ΔH_c and ΔS_c) obtained from the DSC thermograms for the copolymers are listed in **Table 4**. The T_c values initially decrease on increasing the **AMPS** mol fraction before reaching a limiting value at around x_{AMPS} = 0.3 (see **Figure 5a**). The values in **Table 4** also suggest simultaneous reductions of ΔH_c and $\Delta S_c/R$ for the copolymers, at least for low **AMPS** concentrations.

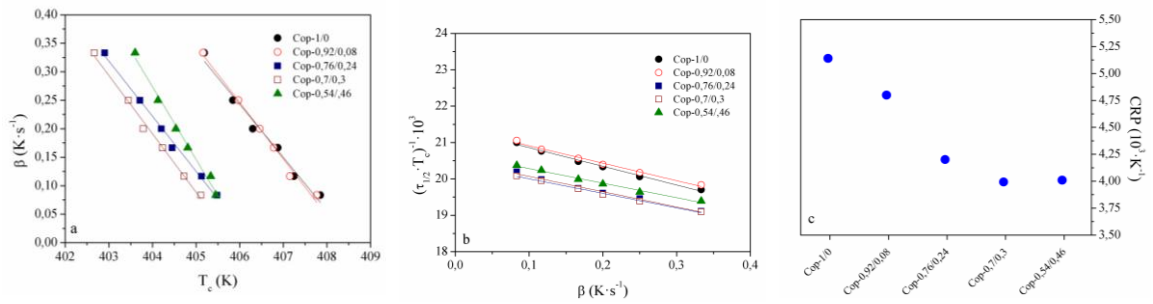

Figure 5. (a) T_c values; (b) $\tau_{1/2}$; (c) ξ values (**Eq. 2**) for the **10-MeOAzB/AMPS** copolymers:

The non-isothermal isotropic-smectic A phase transition of the copolymers was analysed using the same methodology described for the **P10-MeOAzB** homopolymer. The dependence of X_t on $\phi(t)$ for the phase transition of the copolymers cooled at β = 5 and 20 ºC·min^{-1} is shown in **Figure 4b**. These curves are sigmoidal in shape similar to those observed for the homopolymer, and was understood as reminiscent of autocatalytic processes. The **AMPS** mol fraction has a marked effect on both the relative position and the shapes of the X_c curves, suggesting variations in the phase transition process [**10**]. In order to quantify these differences, the kinetics parameters ξ, Δt_c and $\tau_{1/2}$ were calculated for each of the copolymers (**Figure 5b** and **5c**).

The introduction of **AMPS** units causes immediate reduction in the rate of the phase transition, which can be attributed to the introduction of heterogeneities or defects in these random copolymers [**21**]. At higher AMPS concentrations, ξ seems to stabilise until reaching a plateau. These results can be related to the entropy changes calculated for the phase transition and plotted in **Figure 6** as a function of the compositions of the polymers. The remarkable similarity between the evolution of ξ and ΔS_c with composition, and the absence of nematic phases, underpin the role of orientational dynamics on the formation of the smectic A phase from the isotropic melt [**22, 23**].

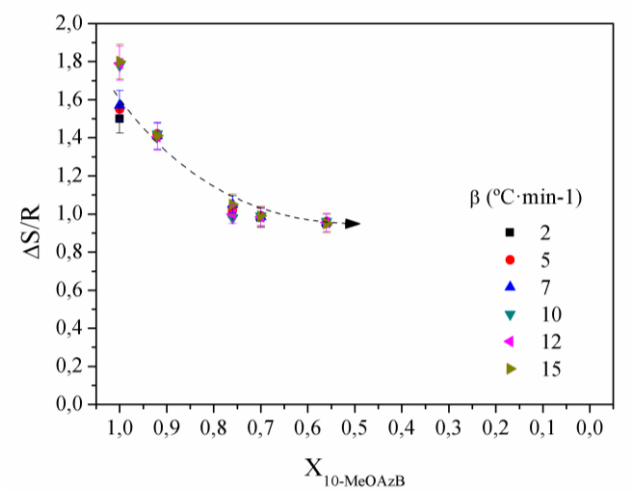

Figure 6. The dependence of the entropy change associated with the isotropic-liquid crystal phase transition ($\Delta S_c/R$) measured for differing cooling rates on the composition of the **10-MeOAzB/AMPS** copolymers. For the homopolymer we see an isotropic-nematic-smectic A transition while the copolymers exhibit an isotropic-smectic A transition

The evaluation of the bulk isotropic-smectic A phase transition of the copolymers was completed by studying the apparent activation energy of the process. The Kissinger and Flynn-Wall-Ozawa models were applied to calculate the apparent activation energies of the phase transition (Ea_{Tc}), from the plots of $\ln(\beta \cdot T_c^{-2})$ and $\log(\beta)$ against T_c^{-1} (**Figure 7a** and **Figure 7b**, respectively). The apparent activation energies obtained by the two methods are similar and are shown in **Figure 7c** as a function of x_{AMPS}. At low **AMPS** concentrations, Ea_{Tc} remains nearly unaltered respect to **P10-MeOAzB** and a sudden increase in the absolute values occurs at $x_{AMPS} > 0.3$.

It is noteworthy in the previous results how the asymptotic behaviour of ξ and ΔS_c coincides with the onset of the Ea_{Tc} increase. This effect occurs at composition ranges when the **10-MeOAzB/AMPS** copolymers exhibit simultaneous formation of acid aggregation and liquid crystalline behaviour ($0.30 \leq x_{AMPS} \leq 0.56$) [**7**]. These results suggest that the combination of entropic and enthalpic effects may promote the forming role of the acid groups in the liquid crystal phase structure of the copolymers and the formation of pronounced microphase separated morphologies.

The shapes of the Ea_{Tc} curves, which resemble exponential behaviour, also suggest that further additions of **AMPS** concentrations would represent a great increase in the activation energy.

Below a certain threshold **10-MeOAzB** concentration, the rate of the phase transition (ξ) is possibly too slow to compensate the high intermolecular interactions in the melt caused by acid aggregation *via* hydrogen bonding. This accounts for the inhibition of the liquid crystallinity observed in the precedent studies for the **10-MeOAzB/AMPS** copolymers with x_{AMPS}>0.56 [**7**].

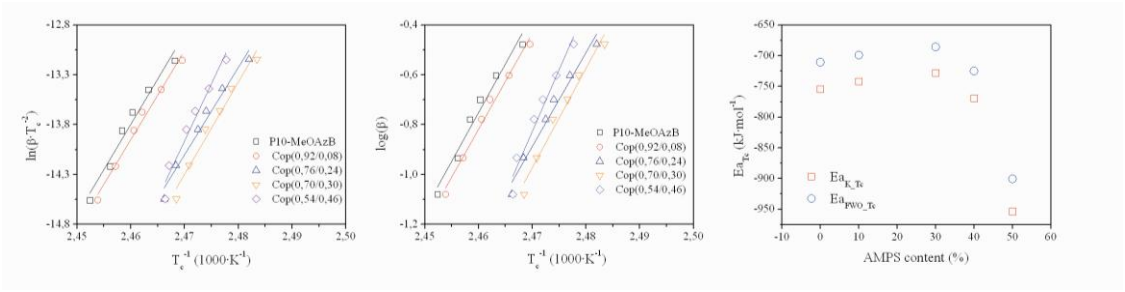

a b c

Figure 7. Calculation of the activation energy of the isotropic-smectic A process for the **10-MeOAzB/AMPS** copolymers (Ea_{Tc}). Plots of the (a) Kissinger, (b) Flynn-Wall-Ozawa methods; (c) Evolution of Ea_{Tc} for the two methods with the composition.

4.2.2 Avrami analysis of the isotropic-smectic A phase transition for the 10-MeOAzB/AMPS copolymers

The phase transition kinetics of the copolymers were further analysed by applying the Avrami equations and following the methodology described for the **10-MeOAzB** homopolymer (**Eq. 5** to **8**). It is possible to see how the copolymers with lower **AMPS** units (**Figure 8a**) clearly show the two linear regions observed for **P10-MeOAzB** (**P1** and **P2** processes in **Figure 3b**). On the other hand, the slopes of the two regions seem to equalise at higher concentrations of **AMPS** (**Figure 8b**). The kinetic parameters of the **P1** and **P2** processes are quantified by calculating the n_i, Z_i *and* k_i values as a function of the cooling rates and copolymer composition, and the results are included in **Table 3**.

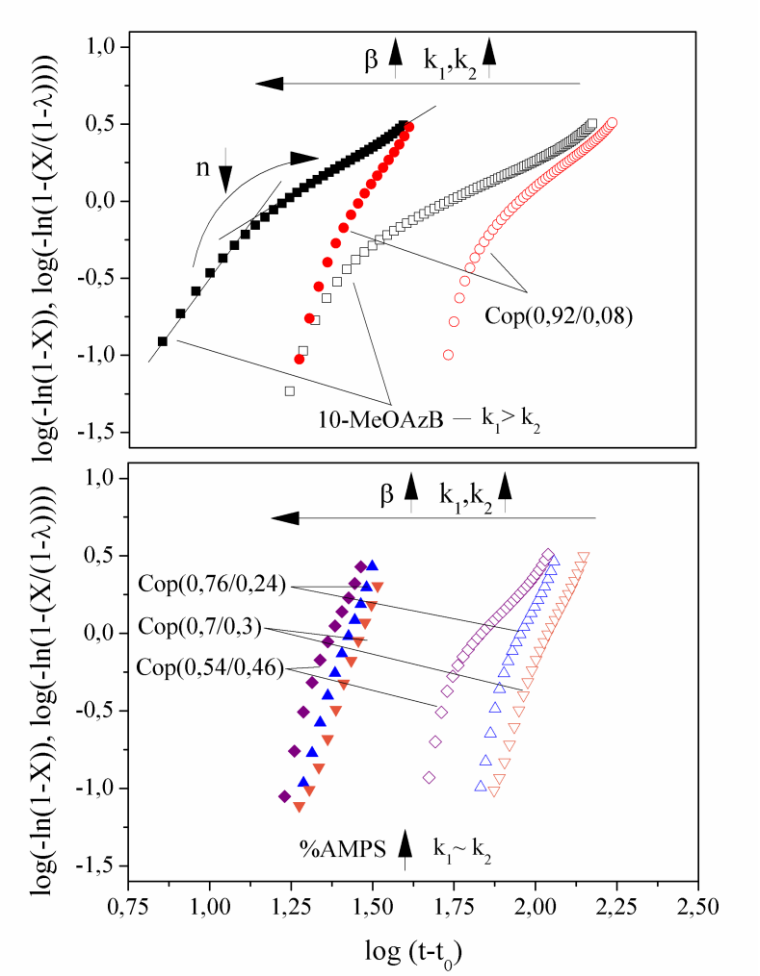

Figure 8. Examples of Avrami plots obtained for the phase transition of the **10-MeOAzB/AMPS** copolymers at high and low cooling rates. High (a) and intermediate (b) 10-MeOAzB concentrations

An increase in the *n* values is observed in the case of the copolymers, respect to the homopolymer, for both processes. This variation could be indicative of a change in the phase transition mechanism by the presence of **AMPS** units, and is in coherence with the absence of the nematic phase in the copolymers observed by microscopy [**11, 25**]. The changes in the slopes observed in the Avrami curves and underlined in **Figure 8** are also reflected in variations of the individual rate constants of **P1** (k_1) and **P2** (k_2). Lower values of k_i are found in the copolymers respect to the homopolymer. This fact agrees with the reduction of the phase transition rate observed through the ξ values by the addition of **AMPS** units (see **Figure 5c**).

Moreover, while $k_1 > k_2$ in the case of **P10-MeOAzB**, $k_1 \approx k_2$ for *Cop(0.7/0.3)* and copolymers with higher AMPS concentrations. *Cop(0.92/0.08)* shows an intermediate behaviour and, finally, a sensitive increase on the k_i values is observed for *Cop(0.54/0.46)*.

The equalising of the constant rates (k_1, k_2) seems to indicate that the two individual processes, clearly visible in the homopolymer (**P1** and **P2**), are merging to a simple transition process for some of the copolymers. **Figure 9** shows a proposed scheme of the LC phase formation from the isotropic melt in the **10-MeOAzB/AMPS** copolymers. The formation of liquid crystal phases usually involves orientational, translational and configurational processes [**22**]. In the case of the homopolymer (**P10-MeOAzB**, **Figure 9a),** the observance of the nematic phase (1D order) denotes an initial *orientation process* over a clear temperature range (**P1**). We can assume that the nematic template is *nucleating* the formation of the smectic layers (2D order) by the presence of pre-orientated mesogens. The smectic templates will then require backbone cooperative *translational processes* and side groups arrangements (to improve packing efficiency in interdigated Smectic phases) (**P2**). Such model fits well to previous findings in methacrylate azo-benzene-based homopolymers [**16**].

In the case of the **10-MeOAzB/AMPS** copolymers, our kinetics results have indicated an initial decrease of the phase transition rate (**Figure 5c**), ascribed to a decrease in the entropy change (**Figure 6**). According to the model proposed in **Figure 9b**, such decrease could be related to partial inhibition of the orientation of the mesogenic units, caused by the inclusion of ionic groups into the LC templates. This view is also consistent with the absence of nematic phases in the copolymers. However, the low concentration of AMPS will still allow for high mobility at long range and for the compression of the backbone to accommodate the non-mesogenic units into LC templates. Thus, it is possible that orientational processes are somehow overcooled and overlapping longer rate translational phenomena, and this may account for the decrease in the bulk phase transition temperature (**Figure 5a**) [**7**]. The recovery of the phase stability observed in the $0.30 \leq x_{AMPS}$ 0.54 range could be then explained by a decrease in the actual concentration of AMPS units present in the LC templates, caused by phase separation. This can also explain the stabilisation of the entropic effects, due to a combination of lower local mobility hindrance and higher backbone compression to require effective packing. In this composition range, moreover, the formation of ionic aggregates may also promote stronger intermolecular interactions in the phase separated morphology. Such increase in enthalpic restrictions may act as structure forming at intermediate and high acid concentrations, and is coherent with the rise in the activation values obtained in this work and an increase in the viscosity of the copolymers

(see **Figure 7c**). At the limit, the interactions will produce strong long-rate restrictions in the translational movements of the main chain, and final inhibition of the smectic behaviour (see **Figure 9c)** [**7**, **26, 27**]**.** This hypothesis is also supported by the increase in the glass transition reported for these copolymers (**Table 2**, [**7**])

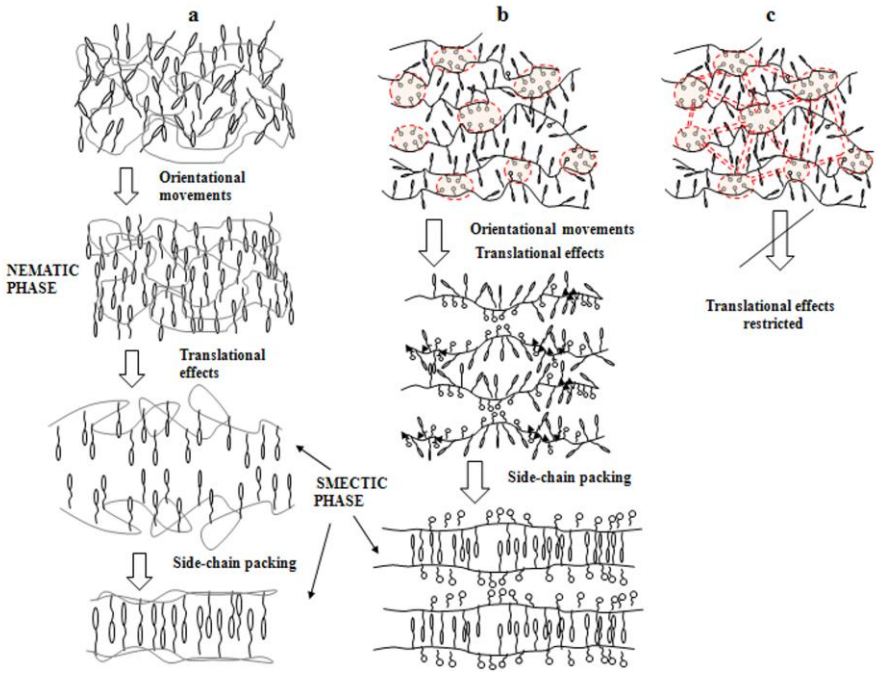

Figure 9. Schematic representation of the isotropic –melt to liquid crystalline transitions in the P10-MeOAzB (a), **P10-MeOAzB/AMPS** copolymers showing liquid crystal behaviour (b) and amorphous **P10-MeOAzB/AMPS** copolymers (c)

4. Conclusions

The introduction of low amounts of acid groups (AMPS) units promotes an initial retardation of the phase transition rate (ξ) of the **10-MeOAzB/AMPS** copolymers, due to a disrupting effect by the introduction of non-mesogenic units into the LC templates. At increasing acid groups concentrations, such destabilisation effects are compensated by a reduction in the effective concentration of AMPS units in the LC regions, driven by the occurrence of phase separation. Further additions of acid groups have structure-forming effects by increasing the rectification of the main chains and the viscosities, attributed to stronger ionic aggregation by hydrogen bonding. At the limit, the mobility restrictions in the backbone are so acute that may produce complete inhibition of the liquid crystal behaviour. In addition, the Avrami analysis showed that overcooling of the orientational processes may be the main reason for phase destabilisation and extinction of the nematic phase in the copolymers, and also for retardation of the phase transition at low acid contents. An equilibrium between entropic and ethalpic effects is achieved at intermediate compositions with phase separated morphologies which allow for simultaneous ionogenic and liquid crystalline behaviours typical of LCI.

1 Shibaev, V.P. Polym. Sci. Ser. A 51 (2009) 1131 – 1193

2 Attard, G.S.; Dave, J.S.; Wallington, A.; Imrie, C.T.; Karasz, F.E. Makromol. Chem. 192 (1991) 1495 - 1508

3 Craig, A.A.; Imrie, C.T.J. Polym. Sci. Polym. Chem. Ed. 34 (1996) 421 - 428

4 Cook, A.G.; Imrie, C.T. Mol. Cryst. Liq. Cryst. 332 (1999) 189 - 198

5 Pebalk, D.A.; Barmatov, E.B.; Shibaev, V.P. Russian Chem. Rev. 74 (2005) 555-576

6 Martínez-Felipe, A. Liq. Cryst. 38 (2011) 1607–1626

7 Martinez-Felipe, A.; Lu, Z.B.; Henderson, P.A.; Picken, S.J.; Norder, B.; Imrie, C.T.; Ribes-Greus, A. Synthesis and characterisation of side chain liquid crystal copolymers containing sulfonic acid groups, submitted to Polymer

8 Avrami, M. J. Chem. Phys. 7 (1939) 1103

9 Avrami, M. J. Chem. Phys. 8 (1940) 212

10 Mandelkern, L. Crystallization of Polymers, 2nd ed.; Cambridge, University Press: Cambridge, UK, 2002; Chapter 8

11 Craig, A.A.; Imrie, C.T. J. Mater. Chem. 4 (1994) 1705-1714

12 Kissinger, H.E. Analytical Chemistry 29 (1957) 1702 - 1706

13 Flynn, J. H.; Wall, L.A. Journal of Polymer Science 4 (1966) 323 – 342

14 Ozawa, T. Journal of Thermal Analysis 2 (1970) 301

15 Mandelkern, L. Crystallization of Polymers, 2nd ed.; Cambridge, University Press: Cambridge, UK, 2002, p 228

16 Cook, A.G., R.T. Inkster, A. Martinez-Felipe, A. Ribes-Greus, I.W. Hamley, C.T. Imrie, Homopolymer Synthesis and phase behaviour of a homologous series of polymethacrylate-based side-chain liquid crystal polymers, submitted for publication to European Polymer Journal

17 Zhu, X.Q., Liu, J.H.; Liu, Y.X.; Chen, E.Q. Polymer 49 (2008) 3103 – 3110

18 Supaphol, P.; Dangseeyun, N.; Srimoaon, P. Polymer Testing 23 (2004) 881

19 Jiang, C.; Wang, D.; Zhang, M.; Li, P.; Zhao, S. European Polymer Journal 46 (2010) 2206–2215

20 Cheng, S.Z.D. Phase transitions in polymers, Ed. Elsevier Jordan Hill, Amsterdam, 2008, pp. 38

21 Mandelkern, L. Crystallization of Polymers, 2nd ed.; Cambridge, University Press: Cambridge, UK, 2002; Chapter 8, pp 265

22 Cheng, S.Z.D. Phase transitions in polymers, Ed. Elsevier Jordan Hill, Amsterdam, 2008, pp. 27

23 Wunderlich, B.; Grebowicz, J. Adv. Polym. Sci. 60 (1984) 1 - 59

24 Cheng, S.Z.D. Phase transitions in polymers, Ed. Elsevier Jordan Hill, Amsterdam, 2008, pp. 25, 37

25 Botines, E.; Puiggalí, J. Eur. Polym. J. 42 (2006) 1595 - 1608

26 Zhao, Y.; Lei, H. Macromolecules 27 (1994) 4525

27 Eisenberg, A.; Hird, B.; Moore, R.B. Macromolecules 23 (1990) 4098

6. Acknowledgments

The authors would like to acknowledge the Spanish Ministry of Science and Innovation, through the Research Projects ENE2007-67584-C03, UPOVCE-3E-013, ENE2011-28735-C02-01, IT-2009-0074 and three FPI and FPU pre-doctoral grants, and the financial support of the Generalitat Valenciana, through the Grisolia and Forteza programs and the ACOMP/2011/189 program. The Vice-rectorate for Research of UPV is also thanked for additional support through the PAID 05-09-4331 and PAID 06-11-2037 projects.

A kinetic study of the formation of smectic phases in novel liquid crystal ionogens

[1]A. Martínez-Felipe; [1]J.D. Badía, [1]L. Santonja-Blasco; [2]C.T. Imrie; [1,*]A. Ribes-Greus

[1]Institute of Materials Technology, Universitat Politècnica de València, Camino de Vera S/N, 46022 Valencia, Spain

[2]Chemistry, School of Natural and Computing Sciences, Meston Building, University of Aberdeen, Aberdeen AB24 3UE Aberdeen, Scotland (UK).

*corresponding author: A. Ribes-Greus, e-mail: aribes@ter.upv.es

Abstract

The non-isothermal kinetic analysis of the isotropic-melt to liquid crystalline phase transition of novel liquid crystalline ionogenic copolymers, LCI, the 10-(4-methoxyazobenzene-4'-oxy)decyl methacrylate]-co-2-(acrylamido-2-methyl-1-propanesulfonic acid)s, **10-MeOAzB/AMPS**, copolymers, has been performed based on calorimetric experiments at different cooling rates. A classical non-isothermal crystallisation methodology, based on Avrami's equations, was applied and it has shown that the formation of the mesophases from the isotropic state occurred close to the thermodynamic equilibrium and can be described with high accuracy by using different kinetic parameters. The results evidence the presence of several individual processes in the formation of liquid crystalline phases from the melt and a strong dependence of phase transition rates and activation energies with acid contents. In addition, the decrease in the phase transition rate is related to a decrease in orientational entropy and the final inhibition of the liquid crystal behaviour is ascribed to an exponential increase in the activation energy of the phase transition, promoted by strong acid aggregation. An optimum composition of the 10-MeOAzB/AMPS copolymers to achieve the dual characteristics of LCI (ionogenic and liquid crystalline behaviour) requires acid concentrations capable of promoting structure-forming effects on the LC phases and the evolution of phase separated morphologies.

Keywords

Liquid crystal polymers (LCP), Differential scanning calorimetry (DSC), non-isothermal melt-crystallisation kinetic analysis

1. Introduction

Side chain liquid crystal polymers (SCLCP) exhibit a unique duality of properties combining those of low molar mass liquid crystals with those of polymers. This combination of properties arises from the structure of SCLCPs in which the mesogenic groups are covalently attached as pendants to a polymer backbone *via* a flexible spacer. The role of the flexible spacer is to decouple, at least to some extent, the relative tendencies of the mesogenic groups to self-assemble and form the liquid crystal phase from those of the polymer backbone to adopt random coil configurations [**1**]. The incorporation of nonmesogenic units along the backbone allows for additional functionalities to be endowed upon the polymer [**2-4**] Of particular interest in recent years have been SCLCPs containing ionic and ionogenic units and these are also referred to as liquid crystal ionomers and iononogens (LCI). This interest stems not only from their considerable application potential in a range of quite diverse areas but perhaps most notably as anisotropic electrolytes, but also because they provide a demanding challenge to our understanding of self-assembly in polymeric systems [**5, 6**].

We recently reported the synthesis and phase behaviour of the 10-(4-methoxyazobenzene-4'-oxy)decyl methacrylate]-co-2-(acrylamido-2-methyl-1-propanesulfonic acid)s, copolymers (**1**),

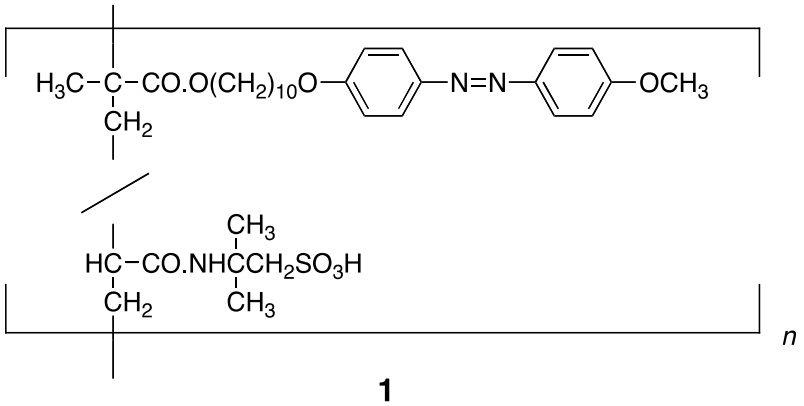

1

and refer to them using the acronym **10-MeOAzB/AMPS** in which 10-MeOAzB refers to the liquid crystal side chain and AMPS to the sulfonic acid-based group. These copolymers exhibited smectic A phase behaviour over a broad range of compositions, specifically for copolymers containing 0.45 or greater mol fraction of 10-MeOAzB side chains [**7**]. This observation, in itself, is not unusual and may be accounted for by a compression of the backbone in the plane perpendicular to the liquid crystal director which enhances the

interactions between the mesogenic groups. Surprisingly, however, the smectic A-isotropic transition did not simply decrease on increasing the AMPS mol fraction but instead appeared to reach a limiting value. Such effect was accompanied by changes in the structure of the smectic A phase on increasing the AMPS mol fraction and this was attributed, at least in part, to hydrogen bonding between the sulfonic acid groups. In addition, a phase separated structure was observed consisting of regions of smectic A phase and acid-rich domains.

It appears therefore that the sulfonic acid groups play a central structure-forming role in determining the phase behaviour of these copolymers. Due to the relevance that processing conditions may have on the preparation of materials and membranes with liquid crystalline templates from the melt, this work investigates with more detail the structural formation of the smectic A phase from the isotropic melt for the **10-MeOAzB/AMPS** copolymers. To achieve this we performed a calorimetric kinetic study of the non-isothermal isotropic melt-liquid crystal phase transition for the homopolymer (**P10-MeOAzB**) and the **10-MeOAzB/AMPS** copolymers. A classical non-isothermal crystallisation approach has been used, based on Avrami's equations and methods [**8, 9, 10**]. We note that such characterisation technique may be successful to determine accurately the lower enthalpy/entropy changes occurring during the transitions from the isotropic state to the mesophases and also between mesophases in low-ordered liquid crystal phases (such as nematic or some smectic phases) [**11 – 22**].

2. Experimental

The synthesis of the 10-MeOAzB/AMPS copolymers was performed by free radical copolymerisation of the monomers, using 1,1'-azobis(cyclohexane carbonitrile) as the initiator in dimethyl formamide (DMF), as has been described in detail elsewhere [**7**, **11**]. The isotropic melt-liquid crystal transition kinetics were investigated using differential scanning calorimetry (DSC), by means of non-isothermal linear temperature-time programs. The DSC thermograms were obtained using a Mettler Toledo DSC 822^e analyser (Columbus, OH, USA) and samples of around 5 mg. The thermal program consisted of alternating heating and cooling scans. An initial heating scan from 25 to 180ºC was applied to ensure the sample had entered the isotropic phase so deleting any thermal history. Subsequently, the samples were submitted to alternating cooling scans (with rate β = 5, 7, 10, 12, 15 and 20 ºC·min^{-1}) and heating scans (with rate β = 10 ºC·min^{-1}) between 0 and 180 ºC. All the thermograms were obtained under a nitrogen atmosphere and using an intracooler for temperature control (Haake EK90/mt). The STAR^e 9.2 software was used to obtain the experimental calorimetric parameters. All the experiments were performed at least three times and the averages and standard deviations of the thermodynamic parameters were obtained.

DSC Phenomenological analysis [10]

The isotropic-liquid crystal phase transitions of the copolymers were analysed using the methodology and equations shown in **Figure 1**. First, the specific enthalpy change associated with the isotropic-liquid crystal phase transition was calculated by integrating the DSC curves obtained in the cooling scan along the time axis (ΔH_t). The fraction of liquid crystal phase at time t (X_t) was obtained by normalising the ΔH_t, values with respect to the enthalpy change corresponding to the complete isotropic-liquid crystal transition (ΔH_∞), following **Eq 1**, ranging from X_{t-0}= 0 (isotropic phase) to $X_{t-\infty}$ = 1 (liquid crystal phase). The half-time of the formation of the liquid crystal phase ($\tau_{1/2}$) was defined as the time at which X_t = 0.5. The phase transition temperature (T_c) was taken to be the minimum of the exotherm. The phenomenological analysis was completed by calculating the so-called phase transition rate parameter, ξ, which in this case actually corresponds to the rate of formation of the liquid crystal phase, defined as the slope of the plots of the variable $(\tau_{1/2} \cdot T_c)^{-1}$ against the cooling rate, β (**Eq. 2**).

Kinetic analysis of the isotropic-liquid crystal phase transition

The study of the bulk isotropic-liquid crystal phase transition of the copolymers was completed by calculating the apparent activation energy (Ea_{Tc}). The Kissinger [**12**] and the Flynn-Wall-Ozawa [**13, 14**] integral methods were applied at the maximum rate of the formation of the liquid crystal phase. The values of $\ln(\beta \cdot T_c^{-2})$ and $\log(\beta)$, respectively, were represented versus T_c^{-1} (**Eq 3** and **4**, respectively), and Ea_{Tc} was calculated from the slopes of the curves.

In addition, the development of multiple individual processes occurring at the isotropic-liquid crystal transition was investigated by applying Avrami's equations to the X_c data [**8, 9**]. The time-dependent probability of the formation of LC domains during the isotropic-liquid crystal transition can be then described by **Eq. 5** in which t_0 corresponds to the onset of the transition. The logarithmic form (**Eq.6**) allows for a linear fit of the phase transition data versus time. In order to consider the effect of the non-mesogenic units in the copolymers, **Eq. 6** was corrected, to give **Eq. 7**, in which $1-\lambda(\infty)$ is the weight fraction of the polymer potentially liquid crystalline at the termination of the process [**15**]. The parameter $1-\lambda(\infty)$, was calculated as the ratio of the ΔH_∞ values of the copolymers with respect to the homopolymer, at each cooling rate. Two empirical parameters can be obtained from the Avrami analysis for each DSC cooling curve, *Z* and *n*, which describe the mechanism of the isotropic-liquid crystal transition processes. From these values, it is possible to calculate a rate parameter $k = Z^{(1/n)}$ (**Eq. 8**), which describes the speed of the formation of the liquid crystal phase for each individual process.

Figure 1. Schematic representation of the methodology followed for the study of the non-isothermal isotropic-liquid crystal phase transition of the **10-MeOAzB/AMPS** copolymers.

3. Results and discussion

3.1 Kinetic analysis of the isotropic-nematic-smectic A phase transition of the homopolymer P10-MeOAzB (*Cop-1/0*)

Figure 2 shows the non-isothermal isotropic melt-liquid crystal exotherms for the **P10-MeOAzB** homopolymer (*Cop-1/0*) at six different cooling rates. All the DSC traces contain two distinct events: a first order exothermic transition at high temperatures (T_c ~ 134 - 136ºC), associated with the isotropic-nematic phase transition, and a glass transition at lower temperatures (T_g ~ 71 - 74ºC) [**4**]. We have shown previously using polarised optical microscopy and small angle X-ray diffraction that on cooling from the isotropic phase, **P10-MeOAzB** forms a narrow temperature range nematic phase and on further cooling, a smectic phase.

The temperature corresponding to the minimum of the exothermic peak (T_c), and the associated enthalpy (ΔH_c) and entropy (ΔS_c) changes measured at different cooling rates are listed in **Table 1**. The values of T_c, ΔH_c and ΔS_c measured at β = -10 ºC·min^{-1} are in good agreement with those reported elsewhere [**4, 7, 16, 17**]. On increasing the cooling rate, the isotropic-nematic transition exotherm becomes broader and shifts to slightly lower temperatures. The extent of supercooling is reproducible but very small (ΔT < 2ºC) when the cooling rate is varied between 5 and 20ºC/min, suggesting that the transition occurs close to the thermodynamic equilibrium [**10**]. This observation is consistent with a thermodynamically weak transition such as a nematic-isotropic transition.

Figure 2. DSC cooling traces of **P10-MeOAzB** (*Cop - 1/0*) obtained at different cooling rates, β, from 5 to 20 ºC/min.

The quantitative analysis of the non-isothermal isotropic-liquid crystal phase transition of **P10-MeOAzB** involved the calculation of the liquid crystal fraction (X_t) as a function of time, $\phi(t) = t - t_0$, using **Eq. 1**. The dependence of X_t on $\phi(t)$ is shown in **Figure 3a** revealing sigmoidal plots, which can be understood as reminiscent of autocatalytic processes [**10**]. The values of apparent total phase transition period, $\Delta t_c = t_{\phi=0.99} - t_{\phi=0.01}$, and half-phase transition time, $\tau_{1/2}$, were obtained from the X_i curves, and are listed in **Table 2**. **Figure 3a** clearly shows the differences in the transitional process of **P10-MeOAzB** seen on varying the cooling rate. Specifically, the shift of the X_t curves towards smaller $\phi(t)$ values on increasing β and the

correspondingly lower Δt_c and $\tau_{1/2}$ values, reveal that isotropic-liquid crystal phase transition takes place more rapidly at higher cooling rates. Only a slight deviation is noted for β=15 and 20 ºC/min at low ϕ_t. Similar observations are usually explained by more pronounced supercooling at higher cooling rates, promoting polymer crystallisation at temperatures more displaced from equilibrium (T_c^0). It appears reasonable to assume that a similar explanation accounts for the behaviour of the isotropic-liquid crystal phase transition, although we note that the extent of supercooling is small. A value of $\xi = 5.14 \cdot 10^{-3}$ K^{-1} was calculated for **P10-MeOAzB** using **Eq. 2**.

Figure 3. Phenomenological and kinetic analysis of the isotropic-nematic phase transition shown by **P10-MeOAzB**: a) X_t curves; b) Avrami plots.

The Avrami plots for the isotropic-nematic phase transition of **P10-MeOAzB** obtained using **Eq. 5** and **7** are shown in **Figure 3b**. Each of these plots contains two distinct linear regions revealing the occurrence of a primary process (hereinafter, **P1**), at short transition times, and a secondary process (hereinafter, **P2**), at longer times. We suggest that these two processes could be assigned to the isotropic-nematic (**P1**) and nematic-smectic A (**P2**) transitions of the homopolymer, respectively [**16, 17**].

From the logarithmic representations of the two individual curves, the Avrami kinetic parameters related to the primary (*Z1*, *n1*, *k1*) and secondary (*Z2*, *n2*, *k2*) processes were obtained, according to **Eq. 7** and **8**, and are given in **Table 3**. The high R^2 values indicate that the two transition processes are well described by the Avrami model. It is also noteworthy that the Avrami rate constants for **P10-MeOAzB**, k_i, are of the same order of magnitude as seen for anisotropic crystallisable polymers (~10^{-2} s^{-1}) [**18, 19**]. The slightly higher rates and *n* values seen for **P10-MeOAzB** may presumably be attributed to the morphological differences between the formation of ordered crystalline phases and transitions involving mesophases [**20**]. The differences in *n* and ln(Z) for the two processes may be interpreted in terms of differences in the mechanisms associated with **P1** and **P2**. Higher Avrami exponents and rate constants are found for **P1** (*n1 > n2; k1 > k2*), suggesting that the isotropic-nematic transition occurs more rapidly that the nematic-smectic A transition.

3.2 Kinetic analysis of the isotropic-smectic A transition for the 10-MeOAzB/AMPS-*x/y* copolymers

3.2.1 Bulk transition properties

Figure 4 shows the DSC cooling scans of the copolymers recorded at the lowest and highest cooling rates, namely, β = 5 and β = 20 ºC·min^{-1}, distinguishing non-isothermal isotropic melt-liquid crystal transition exotherms and glass transitions, T_g. Phase assignation was carried out on the basis of polarised optical microscopy and small angle x-ray diffraction studies [**7**]. The DSC traces measured at intermediate values of β are essentially identical and fall between these limiting curves.

Figure 4. (a) DSC traces recorded at cooling rates, β = 5 and 20 ºC·min^{-1} and (b) the dependence of X_t on $\phi(t)$ for the **10-MeOAzB/AMPS** copolymers. Experimental points have not been shown for the sake of clarity.

The calorimetric parameters (T_c, ΔH_c and ΔS_c) obtained from the DSC thermograms for the copolymers are listed in **Table 4**. The T_c values initially decrease on increasing the **AMPS** mol fraction before reaching a limiting value at around x_{AMPS} = 0.3 (see **Figure 5a**). The values in **Table 4** also suggest simultaneous reductions of ΔH_c and $\Delta S_c/R$ for the copolymers, at least for low **AMPS** concentrations.

Figure 5. (a) T_c values; (b) $\tau_{1/2}$; (c) ξ values (**Eq. 2**) for the **10-MeOAzB/AMPS** copolymers:

The non-isothermal isotropic-smectic A phase transition of the copolymers was analysed using the same methodology described for the **P10-MeOAzB** homopolymer. The dependence of X_t on $\phi(t)$ for the phase transition of the copolymers cooled at β = 5 and 20 ºC·min^{-1} is shown in **Figure 4b**. These curves are sigmoidal in shape similar to those observed for the homopolymer, and was understood as reminiscent of autocatalytic processes. The **AMPS** mol fraction has a marked effect on both the relative position and the shapes of the X_c curves, suggesting variations in the phase transition process [**10**]. In order to quantify these differences, the kinetics parameters ξ, Δt_c and $\tau_{1/2}$ were calculated for each of the copolymers (**Figure 5b** and **5c**).

The introduction of **AMPS** units causes immediate reduction in the rate of the phase transition, which can be attributed to the introduction of heterogeneities or defects in these random copolymers [**21**]. At higher AMPS concentrations, ξ seems to stabilise until reaching a plateau. These results can be related to the entropy changes calculated for the phase transition and plotted in **Figure 6** as a function of the compositions of the polymers. The remarkable similarity between the evolution of ξ and ΔS_c with composition, and the absence of nematic phases, underpin the role of orientational dynamics on the formation of the smectic A phase from the isotropic melt [**22, 23**].

Figure 6. The dependence of the entropy change associated with the isotropic-liquid crystal phase transition ($\Delta S_c/R$) measured for differing cooling rates on the composition of the **10-MeOAzB/AMPS** copolymers. For the homopolymer we see an isotropic-nematic-smectic A transition while the copolymers exhibit an isotropic-smectic A transition

The evaluation of the bulk isotropic-smectic A phase transition of the copolymers was completed by studying the apparent activation energy of the process. The Kissinger and Flynn-Wall-Ozawa models were applied to calculate the apparent activation energies of the phase transition (Ea_{Tc}), from the plots of $\ln(\beta \cdot T_c^{-2})$ and $\log(\beta)$ against T_c^{-1} (**Figure 7a** and **Figure 7b**, respectively). The apparent activation energies obtained by the two methods are similar and are shown in **Figure 7c** as a function of x_{AMPS}. At low **AMPS** concentrations, Ea_{Tc} remains nearly unaltered respect to **P10-MeOAzB** and a sudden increase in the absolute values occurs at $x_{AMPS} > 0.3$.

It is noteworthy in the previous results how the asymptotic behaviour of ξ and ΔS_c coincides with the onset of the Ea_{Tc} increase. This effect occurs at composition ranges when the **10-MeOAzB/AMPS** copolymers exhibit simultaneous formation of acid aggregation and liquid crystalline behaviour ($0.30 \leq x_{AMPS} \leq 0.56$) [**7**]. These results suggest that the combination of entropic and enthalpic effects may promote the forming role of the acid groups in the liquid crystal phase structure of the copolymers and the formation of pronounced microphase separated morphologies.

The shapes of the Ea_{Tc} curves, which resemble exponential behaviour, also suggest that further additions of **AMPS** concentrations would represent a great increase in the activation energy. Below a certain threshold **10-MeOAzB** concentration, the rate of the phase transition (ξ) is possibly too slow to compensate the high intermolecular interactions in the melt caused by acid aggregation *via* hydrogen bonding. This accounts for the inhibition of the liquid crystallinity observed in the precedent studies for the **10-MeOAzB/AMPS** copolymers with x_{AMPS}>0.56 [**7**].

Figure 7. Calculation of the activation energy of the isotropic-smectic A process for the **10-MeOAzB/AMPS** copolymers (Ea_{Tc}). Plots of the (a) Kissinger, (b) Flynn-Wall-Ozawa methods; (c) Evolution of Ea_{Tc} for the two methods with the composition.

4.2.2 Avrami analysis of the isotropic-smectic A phase transition for the 10-MeOAzB/AMPS copolymers

The phase transition kinetics of the copolymers were further analysed by applying the Avrami equations and following the methodology described for the **10-MeOAzB** homopolymer (**Eq. 5** to **8**). It is possible to see how the copolymers with lower **AMPS** units (**Figure 8a**) clearly show the two linear regions observed for **P10-MeOAzB** (**P1** and **P2** processes in **Figure 3b**). On the other hand, the slopes of the two regions seem to equalise at higher concentrations of **AMPS** (**Figure 8b**). The kinetic parameters of the **P1** and **P2** processes are quantified by calculating the $n_{i,}$ Z_i *and* k_i values as a function of the cooling rates and copolymer composition, and the results are included in **Table 3**.

Figure 8. Examples of Avrami plots obtained for the phase transition of the **10-MeOAzB/AMPS** copolymers at high and low cooling rates. High (a) and intermediate (b) 10-MeOAzB concentrations

An increase in the *n* values is observed in the case of the copolymers, respect to the homopolymer, for both processes. This variation could be indicative of a change in the phase transition mechanism by the presence of **AMPS** units, and is in coherence with the absence of the nematic phase in the copolymers observed by microscopy [**11, 25**]. The changes in the slopes observed in the Avrami curves and underlined in **Figure 8** are also reflected in variations of the individual rate constants of **P1** (k_1) and **P2** (k_2). Lower values of k_i are found in the copolymers respect to the homopolymer. This fact agrees with the reduction of the phase transition rate observed through the ξ values by the addition of **AMPS** units (see **Figure 5c**). Moreover, while $k_1 > k_2$ in the case of **P10-MeOAzB**, $k_1 \approx k_2$ for *Cop(0.7/0.3)* and copolymers with higher AMPS concentrations. *Cop(0.92/0.08)* shows an intermediate behaviour and, finally, a sensitive increase on the k_i values is observed for *Cop(0.54/0.46)*.

The equalising of the constant rates (k_1, k_2) seems to indicate that the two individual processes, clearly visible in the homopolymer (**P1** and **P2**), are merging to a simple transition process for some of the copolymers. **Figure 9** shows a proposed scheme of the LC phase formation from the isotropic melt in the **10-MeOAzB/AMPS** copolymers. The formation of liquid crystal phases usually involves orientational, translational and configurational processes [**22**]. In the case of the homopolymer (**P10-MeOAzB**, **Figure 9a),** the observance of the nematic phase (1D order) denotes an initial *orientation process* over a clear temperature range (**P1**). We can assume that the nematic template is *nucleating* the formation of the smectic layers (2D order) by the presence of pre-orientated mesogens. The smectic templates will then require backbone cooperative *translational processes* and side groups arrangements (to improve packing efficiency in interdigated Smectic phases) (**P2**). Such model fits well to previous findings in methacrylate azo-benzene-based homopolymers [**16**].

In the case of the **10-MeOAzB/AMPS** copolymers, our kinetics results have indicated an initial decrease of the phase transition rate (**Figure 5c**), ascribed to a decrease in the entropy change (**Figure 6**). According to the model proposed in **Figure 9b**, such decrease could be related to partial inhibition of the orientation of the mesogenic units, caused by the inclusion of ionic groups into the LC templates. This view is also consistent with the absence of nematic phases in

the copolymers. However, the low concentration of AMPS will still allow for high mobility at long range and for the compression of the backbone to accommodate the non-mesogenic units into LC templates. Thus, it is possible that orientational processes are somehow overcooled and overlapping longer rate translational phenomena, and this may account for the decrease in the bulk phase transition temperature (**Figure 5a**) [**7**]. The recovery of the phase stability observed in the $0.30 \leq x_{AMPS}$ 0.54 range could be then explained by a decrease in the actual concentration of AMPS units present in the LC templates, caused by phase separation. This can also explain the stabilisation of the entropic effects, due to a combination of lower local mobility hindrance and higher backbone compression to require effective packing. In this composition range, moreover, the formation of ionic aggregates may also promote stronger intermolecular interactions in the phase separated morphology. Such increase in enthalpic restrictions may act as structure forming at intermediate and high acid concentrations, and is coherent with the rise in the activation values obtained in this work and an increase in the viscosity of the copolymers (see **Figure 7c**). At the limit, the interactions will produce strong long-rate restrictions in the translational movements of the main chain, and final inhibition of the smectic behaviour (see **Figure 9c)** [**7**, **26, 27**]**.** This hypothesis is also supported by the increase in the glass transition reported for these copolymers (**Table 2**, [**7**])

Figure 9. Schematic representation of the isotropic –melt to liquid crystalline transitions in the P10-MeOAzB (a), **P10-MeOAzB/AMPS** copolymers showing liquid crystal behaviour (b) and amorphous **P10-MeOAzB/AMPS** copolymers (c)

4. Conclusions

The introduction of low amounts of acid groups (AMPS) units promotes an initial retardation of the phase transition rate (ξ) of the **10-MeOAzB/AMPS** copolymers, due to a disrupting effect by the introduction of non-mesogenic units into the LC templates. At increasing acid groups concentrations, such destabilisation effects are compensated by a reduction in the effective concentration of AMPS units in the LC regions, driven by the occurrence of phase separation. Further additions of acid groups have structure-forming effects by increasing the rectification of the main chains and the viscosities, attributed to stronger ionic aggregation by hydrogen bonding. At the limit, the mobility restrictions in the backbone are so acute that may produce complete inhibition of the liquid crystal behaviour. In addition, the Avrami analysis showed that overcooling of the orientational processes may be the main reason for phase destabilisation and extinction of the nematic phase in the copolymers, and also for retardation of the phase transition at low acid contents. An equilibrium between entropic and ethalpic effects is achieved at intermediate compositions with phase separated morphologies which allow for simultaneous ionogenic and liquid crystalline behaviours typical of LCI.

1 Shibaev, V.P. Polym. Sci. Ser. A 51 (2009) 1131 – 1193

2 Attard, G.S.; Dave, J.S.; Wallington, A.; Imrie, C.T.; Karasz, F.E. Makromol. Chem. 192 (1991) 1495 - 1508

3 Craig, A.A.; Imrie, C.T.J. Polym. Sci. Polym. Chem. Ed. 34 (1996) 421 - 428

4 Cook, A.G.; Imrie, C.T. Mol. Cryst. Liq. Cryst. 332 (1999) 189 - 198

5 Pebalk, D.A.; Barmatov, E.B.; Shibaev, V.P. Russian Chem. Rev. 74 (2005) 555-576

6 Martínez-Felipe, A. Liq. Cryst. 38 (2011) 1607–1626

7 Martinez-Felipe, A.; Lu, Z.B.; Henderson, P.A.; Picken, S.J.; Norder, B.; Imrie, C.T.; Ribes-Greus, A. Synthesis and characterisation of side chain liquid crystal copolymers containing sulfonic acid groups, submitted to Polymer

8 Avrami, M. J. Chem. Phys. 7 (1939) 1103

9 Avrami, M. J. Chem. Phys. 8 (1940) 212

10 Mandelkern, L. Crystallization of Polymers, 2nd ed.; Cambridge, University Press: Cambridge, UK, 2002; Chapter 8

11 Craig, A.A.; Imrie, C.T. J. Mater. Chem. 4 (1994) 1705-1714

12 Kissinger, H.E. Analytical Chemistry 29 (1957) 1702 - 1706

13 Flynn, J. H.; Wall, L.A. Journal of Polymer Science 4 (1966) 323 – 342

14 Ozawa, T. Journal of Thermal Analysis 2 (1970) 301

15 Mandelkern, L. Crystallization of Polymers, 2nd ed.; Cambridge, University Press: Cambridge, UK, 2002, p 228

16 Cook, A.G., R.T. Inkster, A. Martinez-Felipe, A. Ribes-Greus, I.W. Hamley, C.T. Imrie, Homopolymer Synthesis and phase behaviour of a homologous series of polymethacrylate-based side-chain liquid crystal polymers, submitted for publication to European Polymer Journal

17 Zhu, X.Q., Liu, J.H.; Liu, Y.X.; Chen, E.Q. Polymer 49 (2008) 3103 – 3110

18 Supaphol, P.; Dangseeyun, N.; Srimoaon, P. Polymer Testing 23 (2004) 881

19 Jiang, C.; Wang, D.; Zhang, M.; Li, P.; Zhao, S. European Polymer Journal 46 (2010) 2206–2215

20 Cheng, S.Z.D. Phase transitions in polymers, Ed. Elsevier Jordan Hill, Amsterdam, 2008, pp. 38

21 Mandelkern, L. Crystallization of Polymers, 2nd ed.; Cambridge, University Press: Cambridge, UK, 2002; Chapter 8, pp 265

22 Cheng, S.Z.D. Phase transitions in polymers, Ed. Elsevier Jordan Hill, Amsterdam, 2008, pp. 27

23 Wunderlich, B.; Grebowicz, J. Adv. Polym. Sci. 60 (1984) 1 - 59

24 Cheng, S.Z.D. Phase transitions in polymers, Ed. Elsevier Jordan Hill, Amsterdam, 2008, pp. 25, 37

25 Botines, E.; Puiggalí, J. Eur. Polym. J. 42 (2006) 1595 - 1608

26 Zhao, Y.; Lei, H. Macromolecules 27 (1994) 4525

27 Eisenberg, A.; Hird, B.; Moore, R.B. Macromolecules 23 (1990) 4098

6. Acknowledgments

The authors would like to acknowledge the Spanish Ministry of Science and Innovation, through the Research Projects ENE2007-67584-C03, UPOVCE-3E-013, ENE2011-28735-C02-01, IT-2009-0074 and three FPI and FPU pre-doctoral grants, and the financial support of the Generalitat Valenciana, through the Grisolia and Forteza programs and the ACOMP/2011/189 program. The Vice-rectorate for Research of UPV is also thanked for additional support through the PAID 05-09-4331 and PAID 06-11-2037 projects.

Table 1. Parameters obtained from the DSC analysis of **P10-MeOAzB**

Cooling rate β (^{o}C·min^{-1})	**T_g (^{o}C)**	**T_c (^{o}C)**	**ΔH_c (J·g^{-1})**	**ΔH_c (kJ·mol^{-1})**	**$\Delta S_c/R$**	**ΔH_m (J·g^{-1})**
5	72.3	135.7	11.42	5.17	1.52	13.41
7	73.8	135.7	11.33	5.12	1.51	13.65
10	73.5	135.2	12.50	5.65	1.67	13.51
12	72.8	134.9	13.46	6.09	1.80	14.24
15	72.1	134.6	13.26	6.00	1.77	13.82
20	73.5	134.2	13.08	5.92	1.75	13.08

Table 2

Table 2. Phenomenological analysis of the crystallization of the**10-MeOAzB/AMPS** copolymers: ΔT_c and $\tau_{1/2}$ values.

	Cop(1/0) P10-MeOAzB		**Cop (0.92/0.02)**		**Cop (0.76/0.24)**		**Cop (0.70/0.30)**		**Cop (0.54/0.46)**	
Cooling rate β (ºC·min^{-1})	**ΔT_c (ºC)**	**$\tau_{1/2}$ (s)**	**ΔT_c (ºC)**	**$\tau_{1/2}$ (s)**	**ΔT_c (ºC)**	**$\tau_{1/2}$ (s)**	**ΔT_c (ºC)**	**$\tau_{1/2}$ (s)**	**ΔT_c (ºC)**	**$\tau_{1/2}$ (s)**
5	167	571	222	570	229	594	275	598	215	589
7	119	413	163	412	183	429	190	430	144	423
10	73	293	119	292	126	304	135	304	112	300
12	53	246	98	245	100	255	115	255	93	252
15	55	199	84	198	78	206	89	206	77	204
20	47	152	69	151	63	157	70	157	60	155

Table 3

Table 3. Kinetic analysis of the crystallization of the **10-MeOAzB/AMPS** copolymers: fitting parameters corresponding to the Avrami's model.

First process															
	P10-MeOAzB		Cop(0,92/0,08)		Cop(0,76/0,24)		Cop(0,70/0,30)		Cop(0,54/0,46)		P10-MeOAzB	Cop(0,92/0,08)	Cop(0,76/0,24)	Cop(0,70/0,30)	Cop(0,54/0,46)
	$logZ_1$	desv	$logZ_1$	desv	$logZ_1$	desv	$logZ_1$	desv	$logZ_1$	desv	R^2				
5	-7,546	0,341	-17,694	0,960	-20,190	0,759	-13,982	0,246	-15,996	1,258	0,987	0,980	0,992	0,997	0,973
7	-7,377	0,234	-14,754	0,961	-15,653	0,961	-14,022	0,252	-15,043	1,098	0,990	0,971	0,976	0,957	0,977
10	-5,324	0,086	-13,106	0,442	-15,035	0,373	-11,41	0,341	-13,996	0,961	0,995	0,988	0,995	0,992	0,975
12	-5,533	0,143	-12,440	0,360	-13,600	0,116	-10,632	0,302	-14,144	0,751	0,994	0,991	0,999	0,993	0,987
15	-4,416	0,093	-12,560	0,336	-12,493	0,128	-10,007	0,192	-13,236	0,527	0,990	0,993	0,998	0,996	0,989
20	-4,025	0,089	-10,490	0,240	-10,561	0,116	-9,814	0,166	-11,058	0,404	0,992	0,983	0,998	0,996	0,991
	n_1	desv	n_1	desv	n_1	desv	n_1	desv	n_1	desv	k_1 (s^{-1})				
5	5,088	0,275	9,616	0,548	10,459	0,406	6,919	0,128	9,027	0,735	0,033	0,014	0,012	0,010	0,017
7	5,398	0,234	8,452	0,545	8,486	0,537	7,332	0,137	9,184	0,639	0,043	0,018	0,014	0,012	0,023
10	4,274	0,087	8,220	0,298	8,780	0,227	6,667	0,210	8,929	0,634	0,057	0,025	0,019	0,019	0,027
12	4,580	0,118	8,148	0,251	8,662	0,110	6,560	0,198	9,520	0,536	0,062	0,030	0,027	0,024	0,033
15	3,699	0,102	8,340	0,298	8,531	0,121	6,346	0,120	9,082	0,378	0,064	0,031	0,034	0,026	0,035
20	3,604	0,089	7,420	0,184	7,459	0,087	6,718	0,121	8,176	0,314	0,076	0,039	0,038	0,035	0,044

Table 3. Kinetic analysis of the crystallization of the **10-MeOAzB/AMPS** copolymers: fitting parameters corresponding to the Avrami's model (cont.)

Second process															
	P10-MeOAzB		Cop(0,92/0,08)		Cop(0,76/0,24)		Cop(0,70/0,30)		Cop(0,54/0,46)		P10-MeOAzB	Cop(0,92/0,08)	Cop(0,76/0,24)	Cop(0,70/0,30)	Cop(0,54/0,46)
	$logZ_2$	desv	$logZ_2$	desv	$logZ_2$	desv	$logZ_2$	desv	$logZ_2$	desv	R^2				
5	-1,890	0,013	-3,481	0,034	-8,496	0,128	-8,841	0,091	-4,192	0,048	0,998	0,996	0,997	0,996	0,997
7	-1,800	0,013	-3,354	0,045	-7,375	0,114	-9,573	0,092	-4,599	0,050	0,997	0,992	0,996	0,999	0,987
10	-1,882	0,021	-4,236	0,043	-8,853	0,162	-9,733	0,145	-5,894	0,077	0,997	0,997	0,996	0,998	0,995
12	-1,770	0,016	-5,314	0,052	-9,455	0,098	-10,115	0,302	-6,638	0,083	0,995	0,998	0,999	0,981	0,998
15	-1,807	0,022	-5,144	0,053	-12,493	0,169	-10,794	0,192	-6,471	0,061	0,998	0,998	0,996	0,993	0,999
20	-1,649	0,015	-4,633	0,045	-8,3435	0,154	-9,117	0,166	-6,309	0,071	0,998	0,997	0,996	0,994	0,998
	n_2	desv	n_2	desv	n_2	desv	n_2	desv	n_2	desv	k_2 (s^{-1})				
5	1,052	0,014	1,760	0,016	4,344	0,061	4,332	0,044	2,333	0,025	0,016	0,011	0,011	0,009	0,016
7	1,149	0,022	1,802	0,023	3,937	0,059	4,979	0,047	2,769	0,034	0,027	0,014	0,013	0,012	0,022
10	1,319	0,023	2,539	0,024	5,116	0,092	5,675	0,083	3,759	0,047	0,037	0,021	0,019	0,019	0,027
12	1,270	0,031	3,365	0,030	5,974	0,093	6,217	0,262	4,456	0,054	0,040	0,026	0,026	0,024	0,032
15	1,347	0,028	3,298	0,033	8,319	0,116	6,862	0,188	4,364	0,040	0,046	0,028	0,031	0,027	0,033
20	1,336	0,014	3,164	0,032	5,837	0,105	6,226	0,147	4,656	0,051	0,058	0,034	0,037	0,034	0,044

Table 4

Table 4. Parameters obtained from the DSC analysis of the **10-MeOAzB/AMPS** copolymers

	Cop (0.92/0.02)						**Cop (0.76/0.24)**					
Cooling rate β (^{o}C·min^{-1})	**T_g (^{o}C)**	**T_c (^{o}C)**	**ΔH_c (J·g^{-1})**	**ΔH_c (kJ·mol^{-1})**	**$\Delta S_c/R$**	**ΔH_m (J·g^{-1})**	**T_g (^{o}C)**	**T_c (^{o}C)**	**ΔH_c (J·g^{-1})**	**ΔH_c (kJ·mol^{-1})**	**$\Delta S_c/R$**	**ΔH_m (J·g^{-1})**
5	71.3	134.4	10.98	4.78	1.41	11.17	72.4	132.8	7.67	3.04	0.90	8.28
7	71.0	133.9	11.11	4.84	1.43	11.03	73.1	132.0	8.26	3.27	0.97	8.12
10	70.1	133.7	10.96	4.77	1.41	10.91	70.2	131.4	7.87	3.12	0.93	7.96
12	70.7	133.0	10.96	4.77	1.41	10.73	70.2	131.0	7.74	3.06	0.91	7.97
15	71.1	132.1	10.90	4.74	1.41	10.67	70.8	130.5	7.86	3.11	0.93	7.94
20	70.0	132.1	10.88	4.74	1.41	11.33	70.7	129.7	7.79	3.08	0.92	7.94

Table 4. Parameters obtained from the DSC analysis of the **10-MeOAzB/AMPS** copolymers (cont.)

	Cop (0.70/0.30)						**Cop (0.54/0.46)**					
Cooling rate β (^{o}C·min^{-1})	**T_g (^{o}C)**	**T_c (^{o}C)**	**ΔH_c (J·g^{-1})**	**ΔH_c (kJ·mol^{-1})**	**$\Delta S_c/R$**	**ΔH_m (J·g^{-1})**	**T_g (^{o}C)**	**T_c (^{o}C)**	**ΔH_c (J·g^{-1})**	**ΔH_c (kJ·mol^{-1})**	**$\Delta S_c/R$**	**ΔH_m (J·g^{-1})**
5	69.7	132.0	8.56	3.24	0.96	7.46	68.3	132.3	9.13	2.99	0.89	8.26
7	68.5	131.6	7.99	3.03	0.90	7.36	71.1	132.2	8.72	2.85	0.85	8.82
10	70.8	131.1	7.90	2.99	0.89	7.43	71.7	131.6	8.68	2.84	0.84	8.81
12	70.7	130.7	8.08	3.06	0.91	7.31	70.1	131.1	8.74	2.86	0.85	9.20
15	71.0	130.3	8.02	3.04	0.91	7.30	70.9	130.5	8.84	2.89	0.86	9.19
20	71.2	129.4	8.07	3.06	0.91	7.42	70.9	129.9	8.83	2.89	0.86	9.18

Figure 1

Click here to download high resolution image

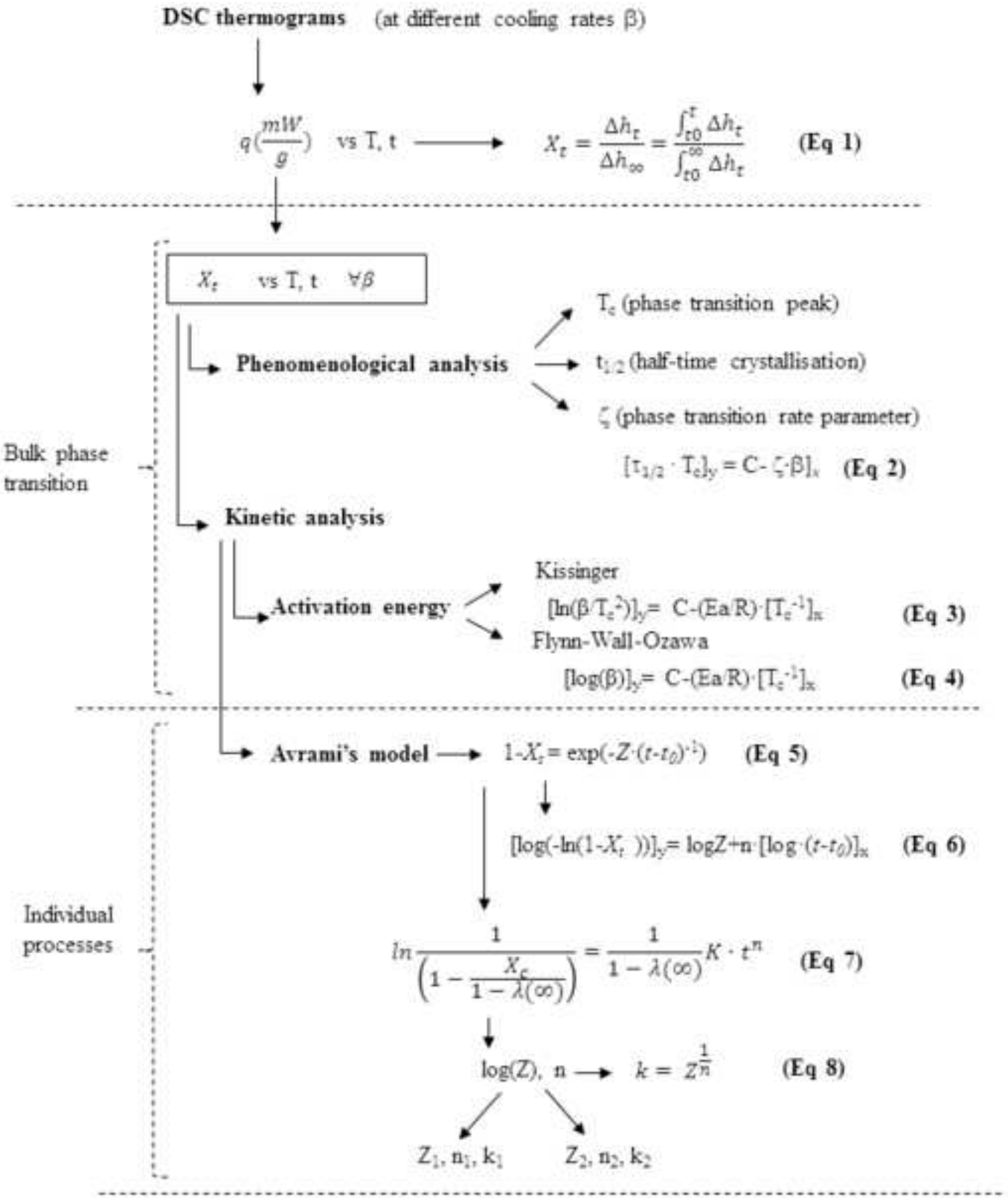

Figure 2

Click here to download high resolution image

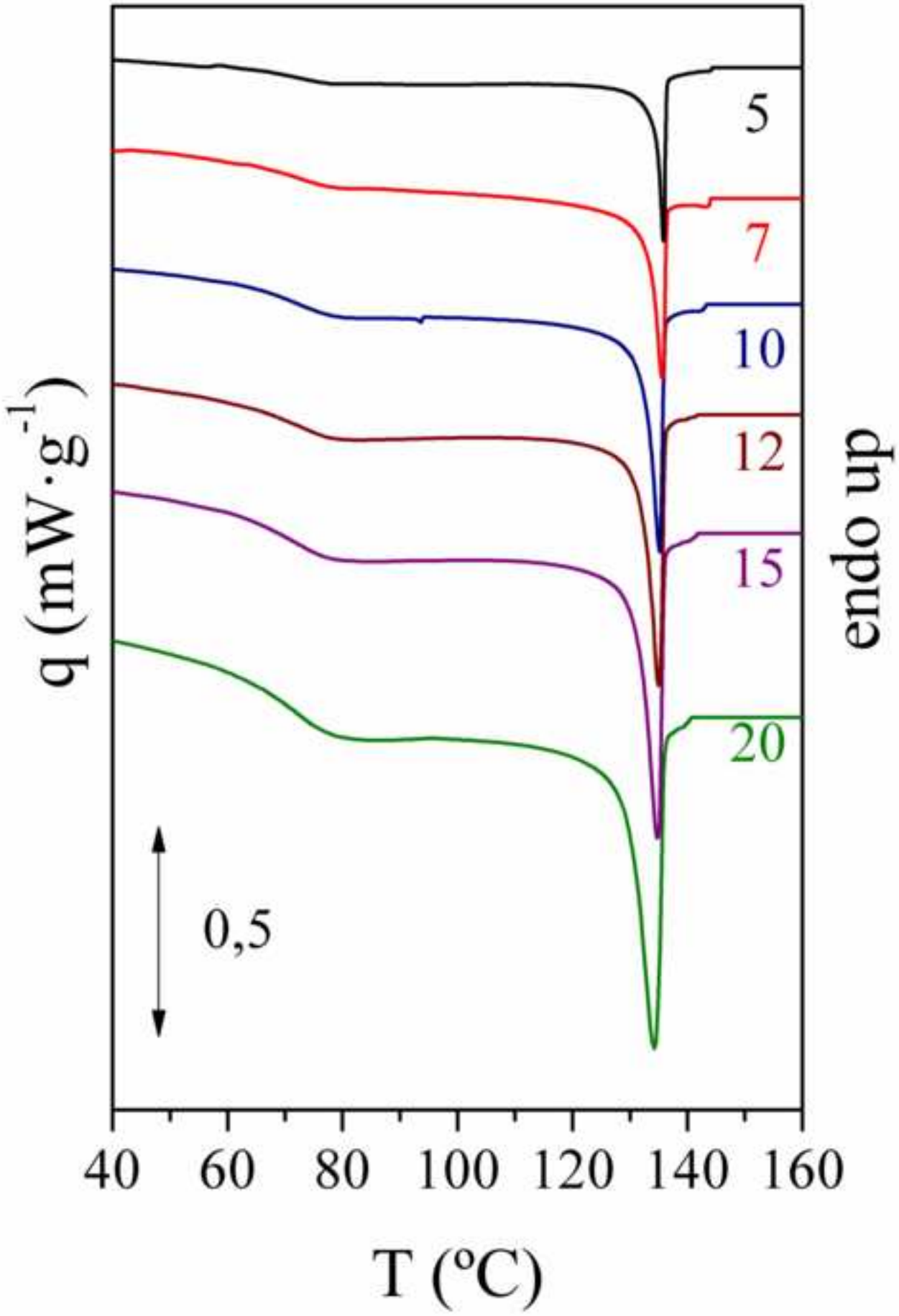

Figure 3a

Click here to download high resolution image

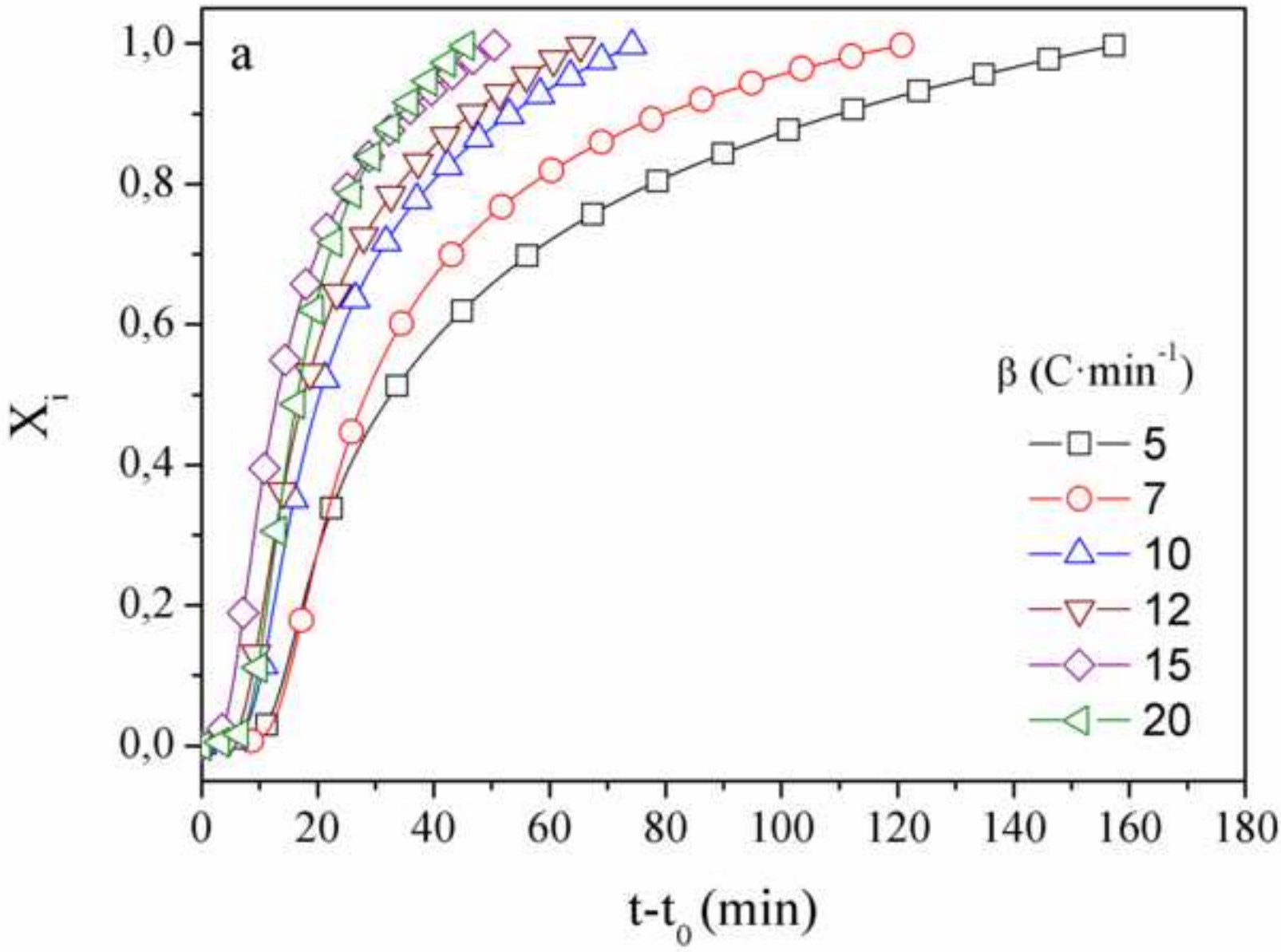

Figure 3b

Click here to download high resolution image

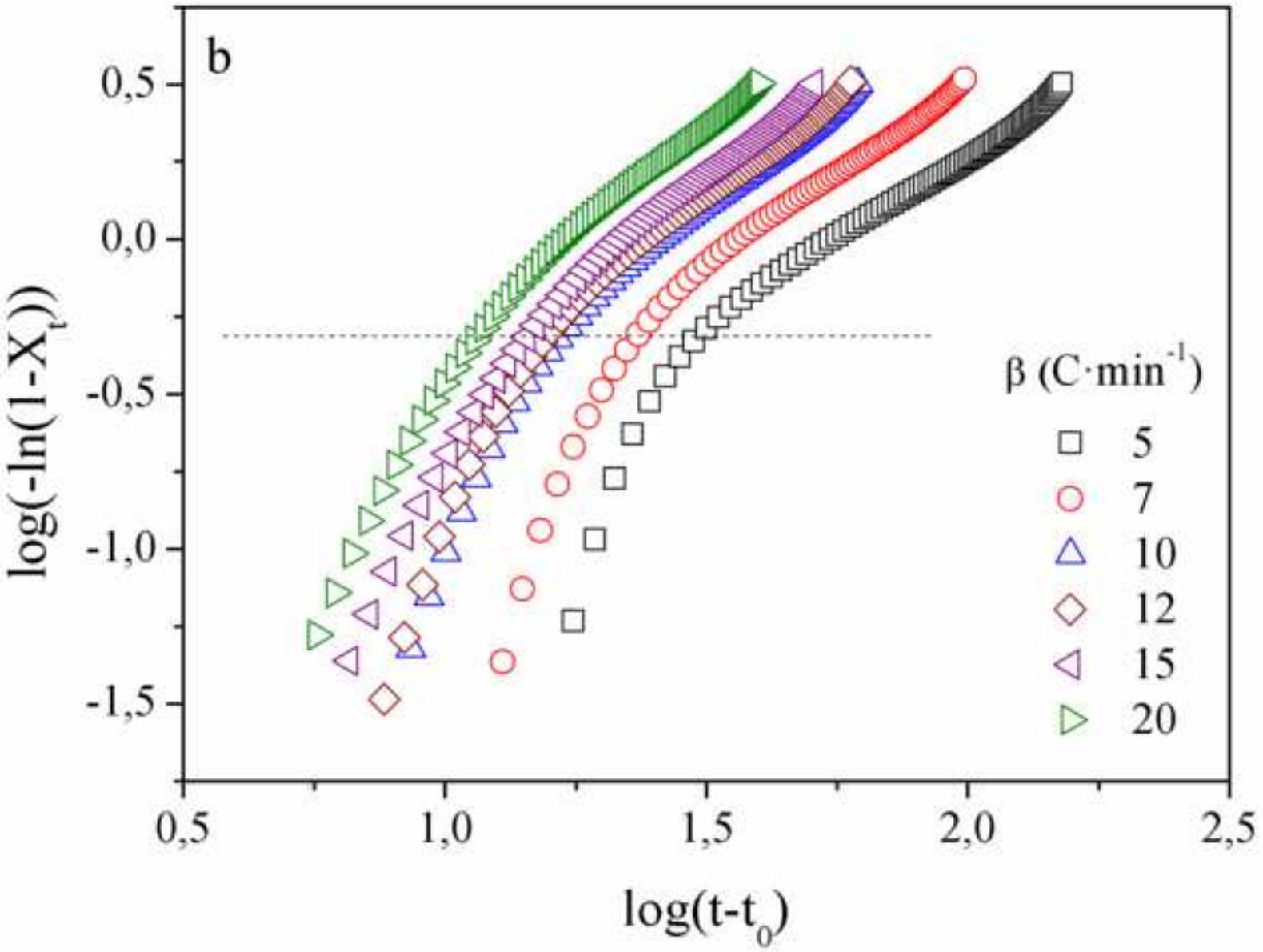

Figure 4a

Click here to download high resolution image

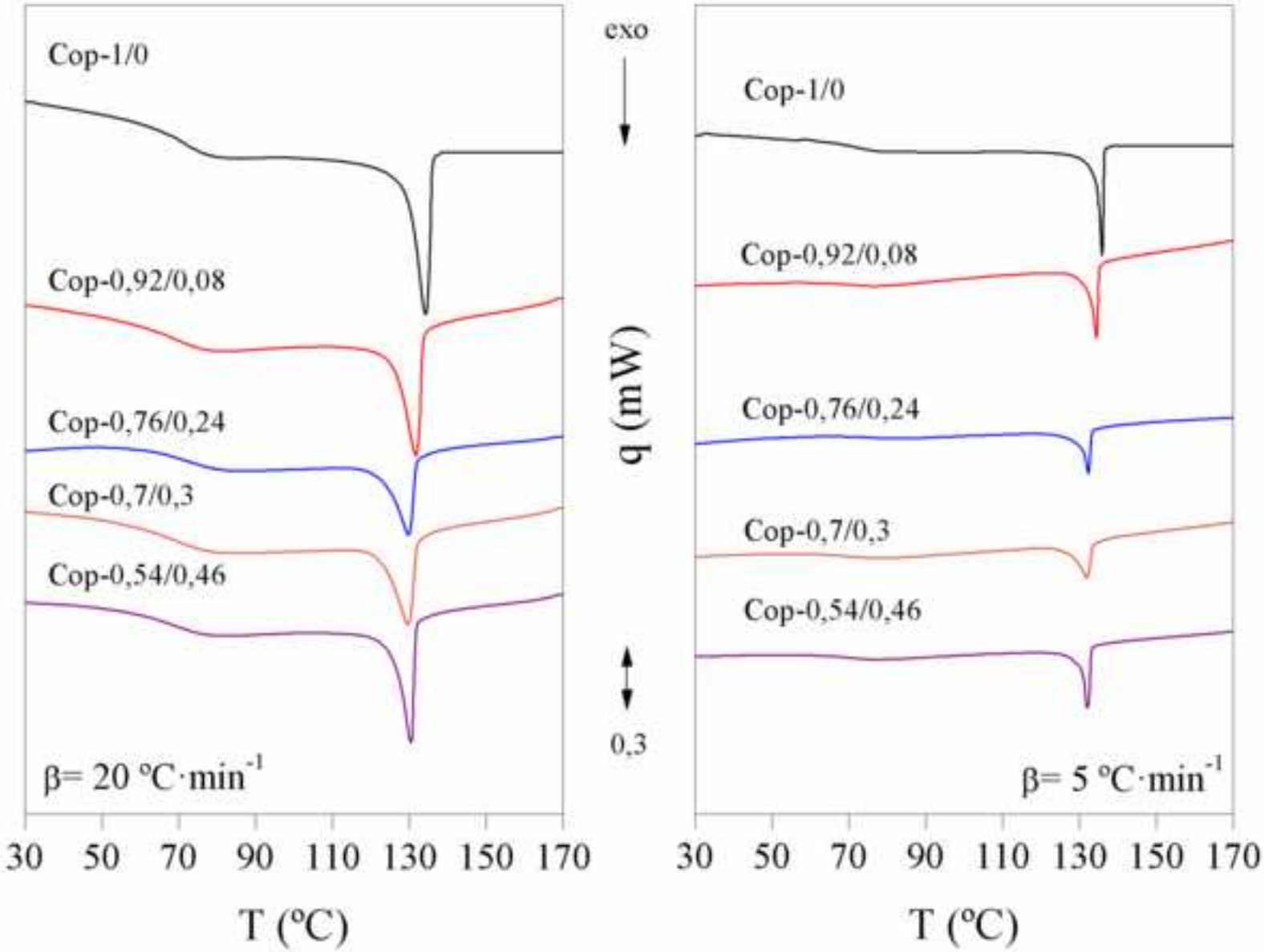

Figure 5a

Click here to download high resolution image

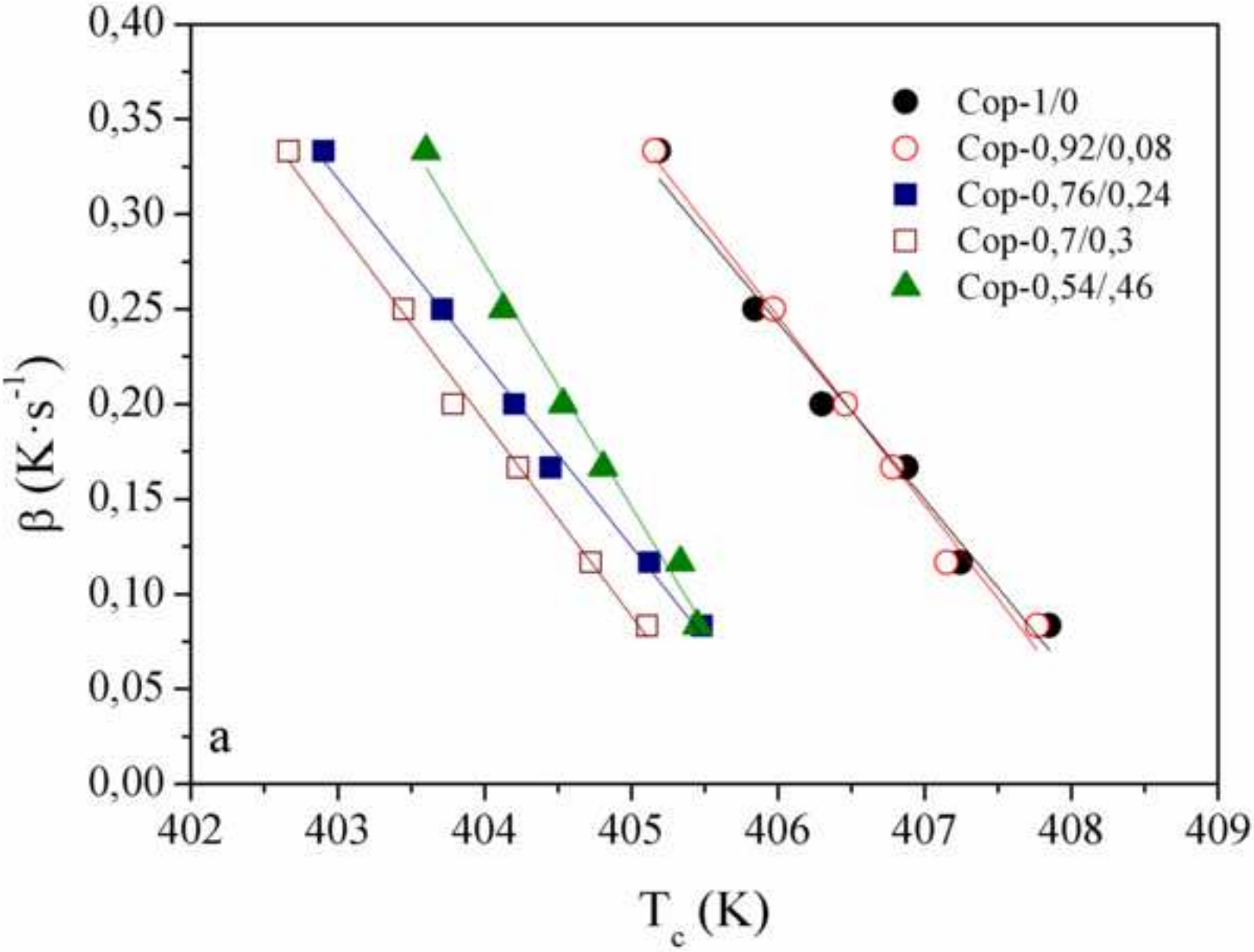

Figure 5b

Click here to download high resolution image

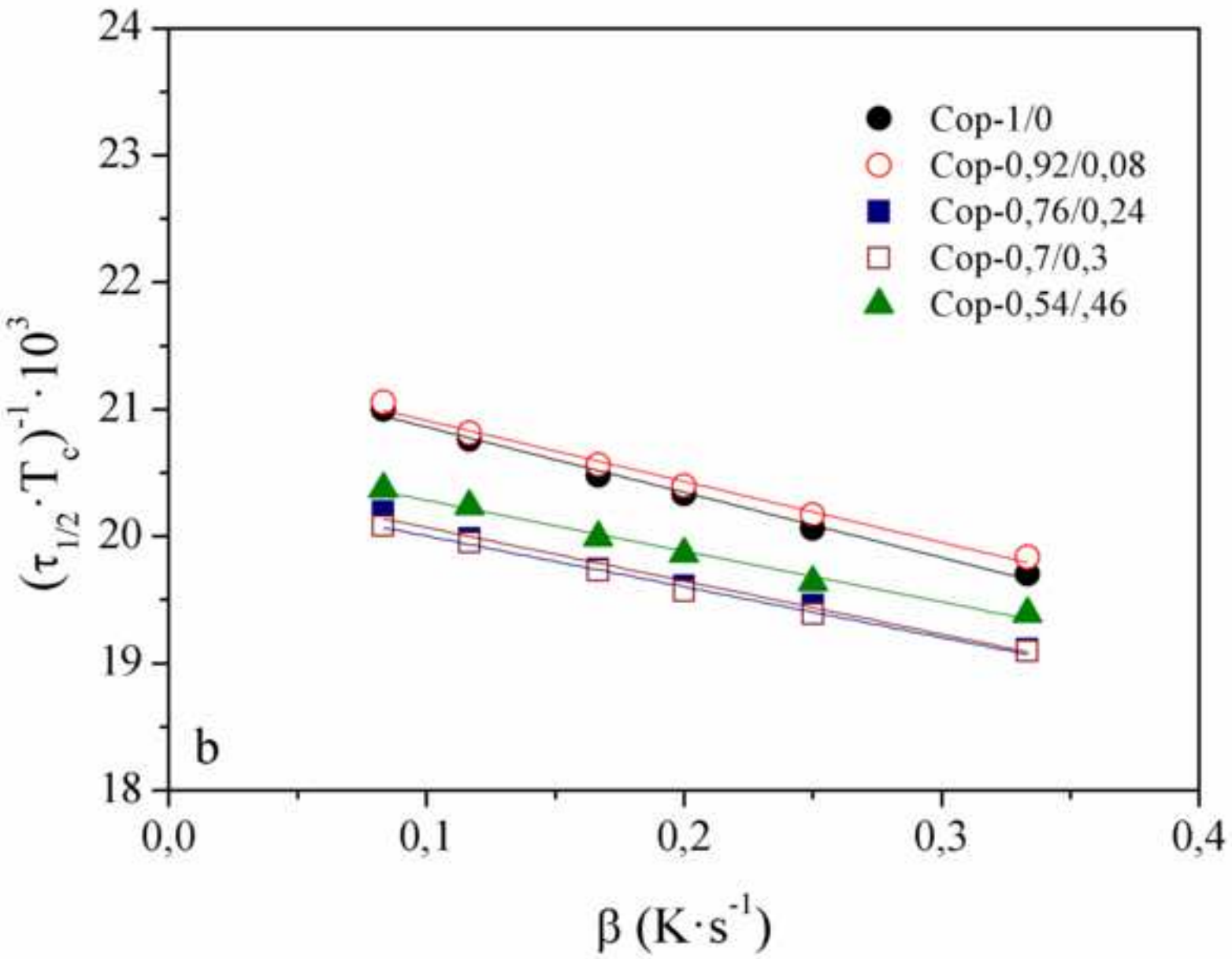

Figure 5c

Click here to download high resolution image

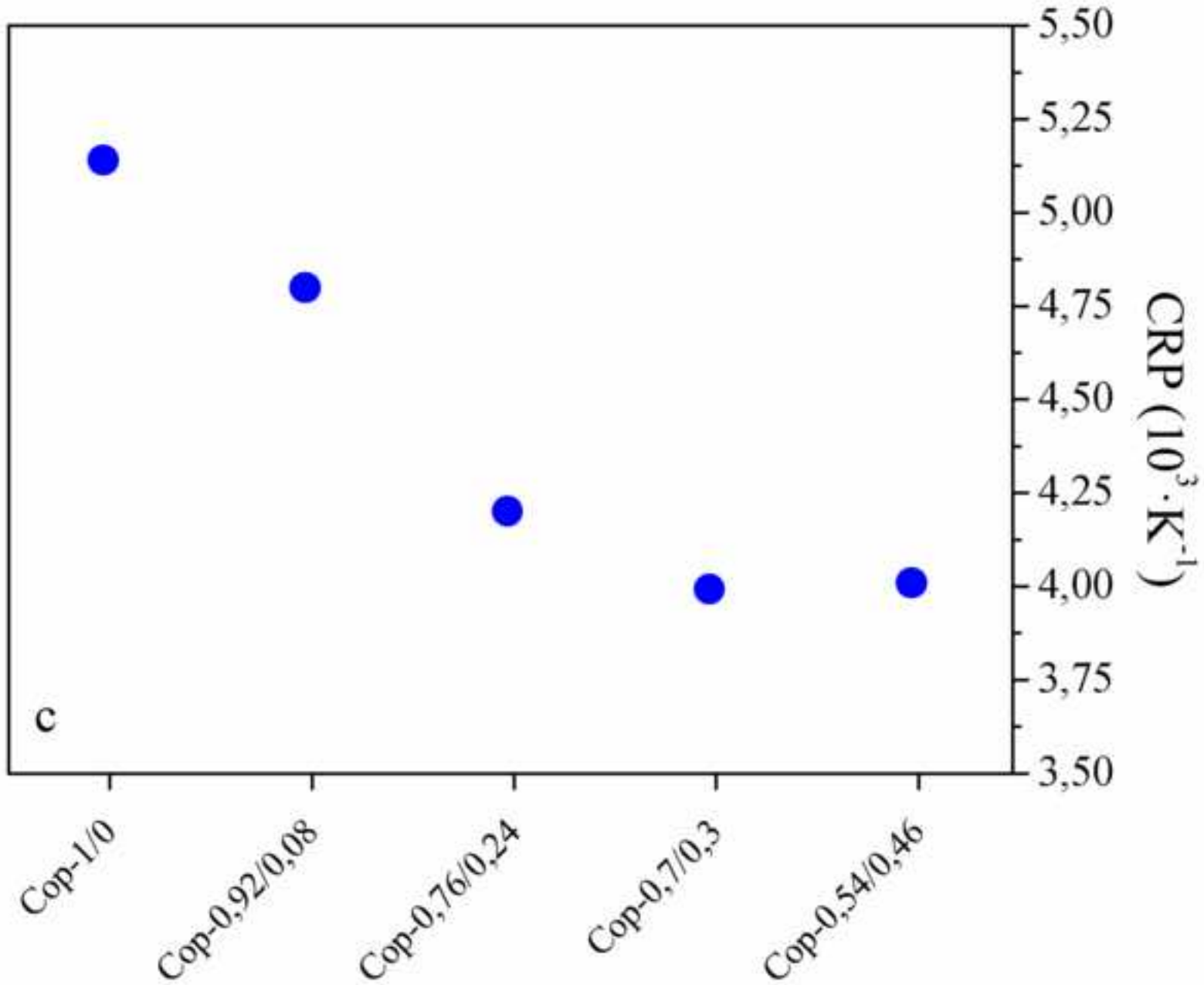

Figure 6

Click here to download high resolution image

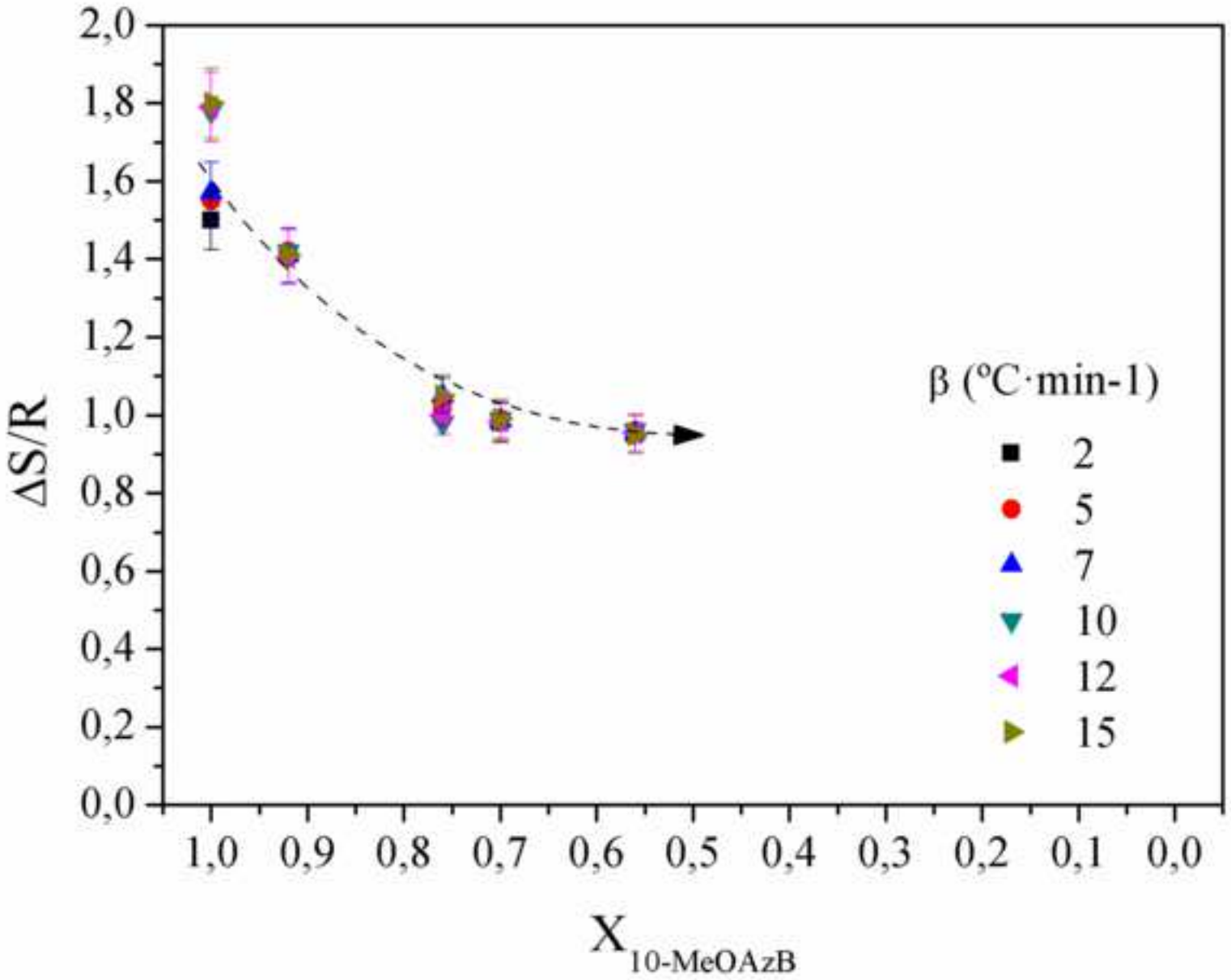

Figure 7

Click here to download high resolution image

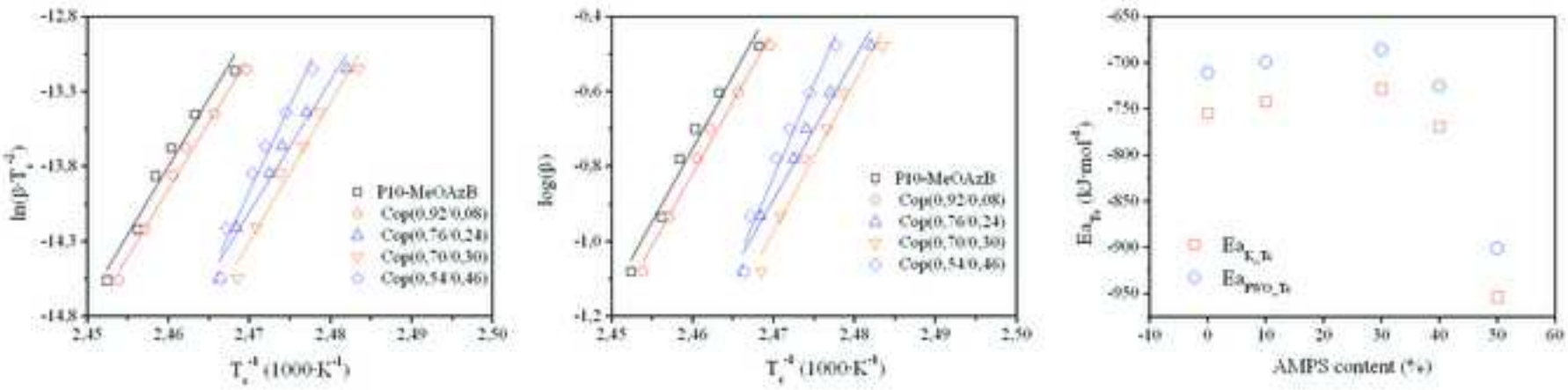

Figure 8

Click here to download high resolution image

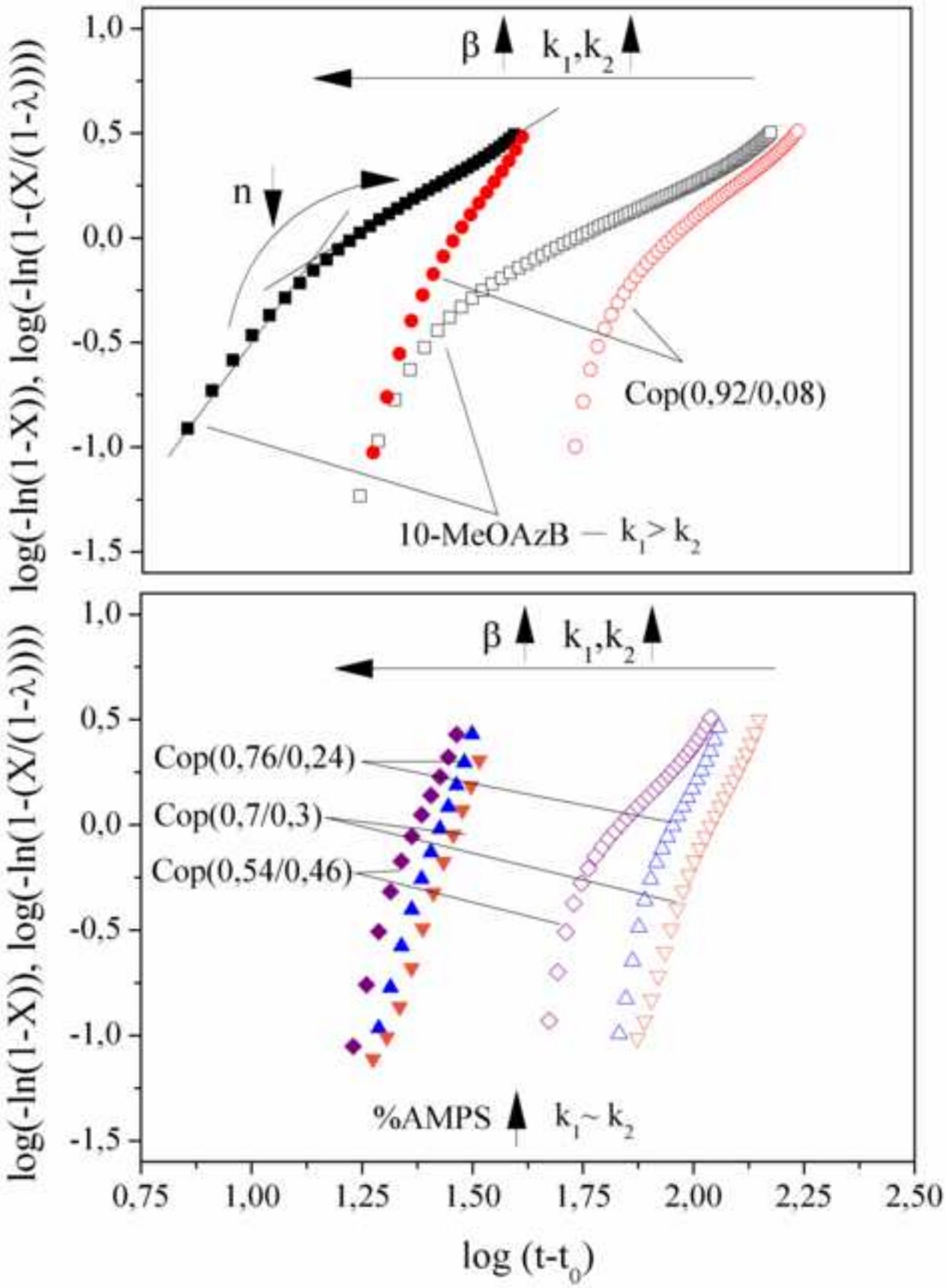

Figure 9

Click here to download high resolution image